Fall 12-2020

A Parametric Analysis of a Turbofan Engine with an Auxiliary Bypass Combustion Chamber – The TurboAux Engine

Kaleab Fetahi
Old Dominion University, kfeta001@odu.edu

A PARAMETRIC ANALYSIS OF A TURBOFAN ENGINE WITH AN AUXILIARY BYPASS COMBUSTION CHAMBER – THE TURBOAUX ENGINE

by

Kaleab Fetahi
B.S. May 2019, Old Dominion University
M.S. December 2020, Old Dominion University

A Thesis Submitted to the Faculty of
Old Dominion University in Partial Fulfillment of the
Requirements for the Degree of

MASTER OF SCIENCE

MECHANICAL ENGINEERING

OLD DOMINION UNIVERSITY
December 2020

Approved by:

Sharan Asundi (Director)

Arthur C. Taylor (Co-Director)

Adem Ibrahim (Member)

ABSTRACT

A PARAMETRIC ANALYSIS OF A TURBOFAN ENGINE WITH AN AUXILIARY BYPASS COMBUSTION CHAMBER – THE TURBOAUX ENGINE

Kaleab Fetahi
Old Dominion University, 2020
Director: Dr. Sharan Asundi

A parametric study of a novel turbofan engine with an auxiliary combustion chamber, nicknamed the TurboAux engine is presented. The TurboAux engine is conceived as an extension of a low-bypass turbofan engine with an auxiliary bypass annular combustion chamber around the core stream. The study presented in this thesis is motivated by the need to facilitate clean secondary burning of fuel at temperatures higher than conventionally realized, from air exiting the low-pressure compressor. The parametric study starts by analyzing the turbojet engine and its performance with and without an afterburner segment attached. Following that, the conventional turbofan and its mixing counterpart are studied, also with and without an afterburner segment. Then, a simple optimization analysis to identify optimal 'fan' pressure ratios for a series of conventional low-bypass turbofan engines with varying bypass ratios (0.1 to 1.5) is done. The optimal fan pressure ratios and their corresponding bypass ratios are adapted to study the varying configurations of the TurboAux engine. The formulation and results are an attempt to make a case for charter aircrafts and efficient close-air-support aircrafts. The results yielded increased performance in thrust augmentation, but at the cost of a spike in fuel consumption. Further analysis is required to determine the application of the TurboAux.

Co-Director: Dr. Arthur C. Taylor

This thesis is dedicated to my family and friends for without the support from you all, I would never reach the heights that I have reached. I continue to strive for you all.

ACKNOWLEDGMENTS

I would like to thank my advisor and my committee for the guidance and instruction they have given me, as well as the department for giving me this opportunity to conduct this research. The countless hours of meeting and support from my committee deserve recognition.

NOMENCLATURE

B	Bypass Ratio	
C	Local Speed of Sound	
C_{p0}	Specific Heat Capacity at Constant Pressure	J/kg·K
D	Diameter	m
f_{actual}	Actual Fuel to Air Ratio of Core Stream	
f_{aux}	Actual Fuel to Air Ratio of Auxiliary Stream	
f_{ideal}	Ideal Fuel to Air Ratio	
f_o	Overall Actual Fuel to Air Ratio of Core and Auxiliary Streams	
Fs	Specific thrust	N·s/kg
H_{rpCO2}	Enthalpy of Reaction of Co2	kJ/kmol
H_{rpf}	Enthalpy of Reaction of Fuel	kJ/kmol
HV	Heating Value of Fuel	J/kg
M_a	Flight Speed	
M_{air}	Molar Mass of Air	kg/kmol
$\dot{m}_{aux}$	Mass Flow of Auxiliary Stream	kg/s
$\dot{m}_{core}$	Mass Flow of Core Stream	kg/s
$\dot{m}_{f1}$	Mass Flow of Fuel into Core Stream	kg/s
$\dot{m}_{f2}$	Mass Flow of Fuel into Auxiliary Stream	kg/s
$\dot{m}_{fdry}$	Total Mass Flow of Fuel without Afterburning	kg/s
$\dot{m}_{fwet}$	Total Mass Flow of Fuel with Afterburning	kg/s
M_{fuel}	Molar Mass of Fuel	kg/kmol
P_0	Stagnation Pressure	Pa
P_a	Ambient Static Pressure	Pa
R	Specific Gas Constant	J/kg·K

T	Thrust	kN
T_0	Stagnation Temperature	K
T_a	Ambient Static Temperature	K
T_p	Static Temperature of The Products of Combustion	K
T_r	Static Temperature of The Reactants of Combustion	K
TSFC	Thrust Specific Fuel Consumption	kg/N·hr
V_a	Velocity of Air at Inlet	m/s
w_{CHP}	Specific Work Required to Drive High-pressure Compressor	J/kg
w_{CLP}	Specific Work Required to Drive Low-pressure Compressor	J/kg
Y_{cc}	Moles of Air Required for Stoichiometric Combustion	
γ	Ratio of Specific Heat at Constant Pressure to Specific Heat at Constant Volume	
η_b	Burner Efficiency	
η_c	Compressor Efficiency	
η_d	Diffuser Efficiency	
η_f	Fan Chute Efficiency	
η_m	Mechanical Efficiency	
η_n	Nozzle Efficiency	
η_o	Overall Efficiency	
η_p	Propulsive Efficiency	
η_t	Turbine Efficiency	
η_{th}	Thermal Efficiency	
π_c	Overall Pressure Ratio	
π_{HP}	High-pressure Compressor Pressure Ratio	
π_{LP}	Low-pressure Compressor Pressure Ratio	

TABLE OF CONTENTS

Page

Page

LIST OF TABLES

Table Page

LIST OF FIGURES

Figure Page

Figure Page

CHAPTER I

INTRODUCTION

Since the invention of the steam engine in the late 17th century, humans have been steadily improving and advancing technologically [1]. With these advancements came a deeper desire to incorporate them in machines that made life easier and travel more convenient. The steam engine saw its applications in the travel industry with the advent of the locomotive making transportation across the country significantly faster than previously possible [1]. Following that was the development of the first automobile which made travel by horse and carriage obsolete. Moving forward, in 1903, the Wright brothers did the seemingly impossible and took flight in the very first operational airplanes [2,3]. From there, the doors of innovation and advancements were opened to furthering the capabilities of airplanes as well as other modes of transportation. To no surprise, airplanes were very appealing to the defense industry as well. Fast forwarding to 1911, the first war plane was used to spy on its enemies: a turboprop plane [2]. The turboprop was the primary engine in use in both commercial flights and fighter planes; this was until the development of the first jet engine [3]. Although its inventor is disputed, the patent for the first turbojet was accredited to Frank Whittle in 1930 [3]. The development of the turbojet led to its adaptation in aircraft and was pivotal in how warfare changed moving forward. As humans do throughout history, scientists researched and experimented ways to make these engines faster and more efficient, thus the development of the turbofan and afterburner, respectively. Continuing this trend, the next generation of scientists are seeking out ways to further optimize the technology currently in use.

Background

The implementation of an afterburner, while significantly increasing thrust production, comes at a high cost in fuel consumption [4]. The process of afterburning itself is inefficient in comparison to the main combustion chamber as the reactants of the combustion process in the afterburner are gases depleted of oxygen from the main combustion chamber [4]. A novel approach to mitigate the issues experienced by afterburner engines is proposed by Asundi and Ali [5]. The authors conceived the idea of having a secondary burner in the bypass stream of a turbofan engine to utilize oxygen-rich air for a more efficient combustion process. Incorporating this auxiliary combustion chamber in the bypass stream allows for much higher combustion temperatures (~2500 K) than the core stream of the engine since the gases will not encounter the turbine blade, potentially causing catastrophic damage [5]. Their analysis was conducted under the assumption that the various components of their engine operated isentropically.

Turbojet

In the text *Gas Turbine Theory* by Cohen, Rogers, and Saravanamuttoo, the authors outline the inner workings, operation, and thermodynamics of a myriad of gas turbine engines such as the turbojet, turbofan, turboprop, and such [4]. Conventional turbojet engines have one stream, which passes through the core of the engine without bypassing any of the components [4]. The core stream is compressed through the various stages of the compressor prior to combustion, then after combustion, is expanded through the various stages of the turbine prior to exhausting through a nozzle [4]. The work required by the compressors to compress the flow is provided by the expansion of the hot gases through the turbine. The spinning of the turbine

blades provides shaft work to the compressors, thus completing the cycle. Figure 1 illustrates the configuration of a common turbojet engine.

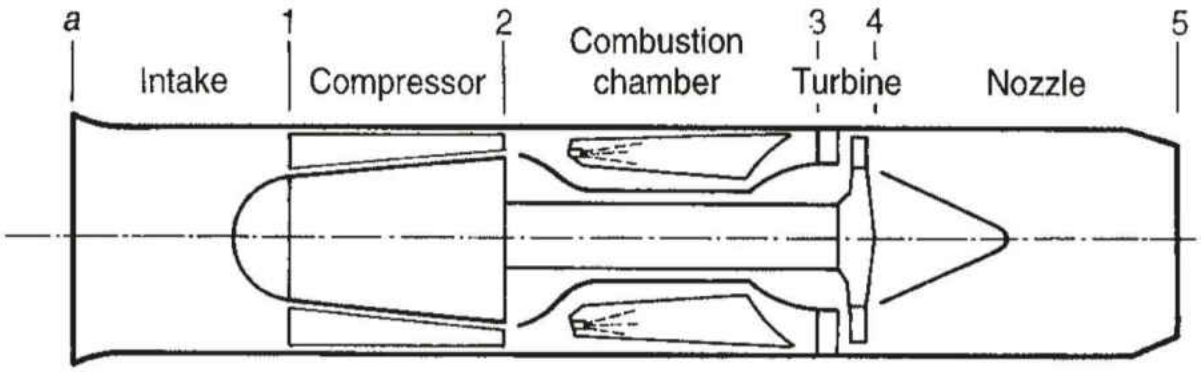

Figure 1. Turbojet Configuration [4]

The core stream, after the combustion stage, has a considerable increase in its thermal and kinetic energy. In current operational engines, there are strict limitations on the temperature that the turbine blades can withstand. Temperatures in excess of 1950 K can cause the thin blades of a turbine to melt, which may damage the engine [4,6]. These limitations manifest in the potential thrust capability of an engine. In an effort to further augment thrust, many different methods have been proposed, but the two most common methods are liquid injection and afterburning [4]. Liquid injection involves injecting a mixture of methanol and water into the inlet of the compressor to cause vaporization of the water which extracts heat from the air resulting in a decrease in compressor inlet temperature [4]. Reheat, or more commonly known as afterburning, is a process in which a segment of the engine prior to the exhaust nozzle, but after the turbine segments, is injected with fuel [4]. The benefit of this method of thrust augmentation is that the absence of the thin turbine blades allows for the products of combustion to be in

excess of 2000K [4]. Figure 2 below shows the T-s diagram for a turbojet engine with reheat at 2000K [4]. The drastic rise in temperature illustrates the drastic fuel consumption in order to reach a stagnation temperature of 2000K.

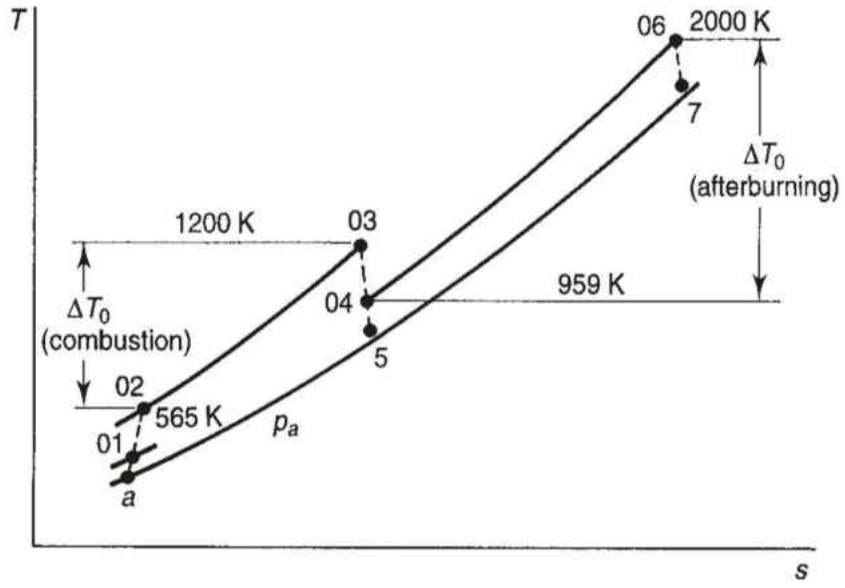

Figure 2. T-s Diagram of a Turbojet with Afterburning [4]

The approximate increase in thrust can be taken as the square root of the ratio between the reheat exit temperature and the reheat inlet temperature [4]. In this specific case, this results in approximately a 44% increase in thrust. Conversely, the increase in fuel consumption can be approximated as the ratio of the sums of the temperature differences in the main combustion cycle and the reheat cycle to the temperature difference in the main combustion chamber. In this specific case, this amounts to approximately a 164% increase in fuel consumption for just a 44% increase in thrust. It is important to note that this might be the case for take-off where the gross thrust and net thrust are equal [4]. Conversely at high cruise velocities, the thrust augmentation is typically well over 100%, and this is due to the fact that for a fixed momentum drag, an increase

in gross thrust relates to significant increase in net thrust [4]. The Concorde, the only supersonic commercial airline, used reheat to accelerate from Mach 0.9 to Mach 1.4 [4]. Despite an increase in fuel flow for a brief period, this jump in net thrust reduced the fuel consumption due to the fast acceleration through the high-drag region around Mach 1.0 [4]. Afterburning offers a considerable amount more thrust augmentation for low-bypass turbofans due to the relatively low temperatures after the hot and cold streams mix [4]. In conjunction with the stream having lower temperatures, it also has more free oxygen for combustion available from the bypass stream than a conventional turbojet with an afterburner [4]. Military turbofans use afterburning for take-off and combat maneuvering [4]. The configuration of a common afterburner segment is shown in figure 3.

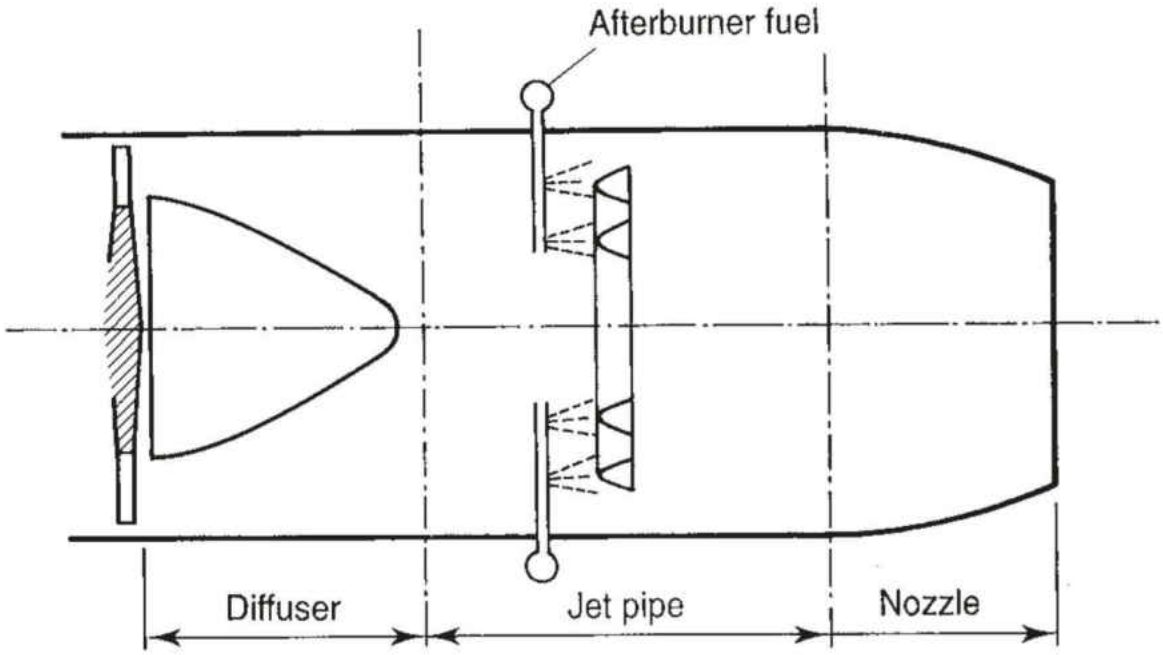

Figure 3. Afterburner Segment Configuration [4]

Turbofan

The conception of the turbofan engine as an extension of the turbojet was originally meant as a means to increase the propulsive efficiency of the turbojet by reducing the mean exit stream velocity thus increasing the fuel efficiency [4]. Another issue the turbojet engine faces is the issue of excess heat from the combustion process. The turbofan engine mitigates this issue by incorporating a bypass stream [4]. This stream passes over the core of the engine and cools its components with air from the inlet. This bypass stream is then exhausted through a separate nozzle. Figure 4 below illustrates the configuration of the conventional commercial two-spool turbofan engine.

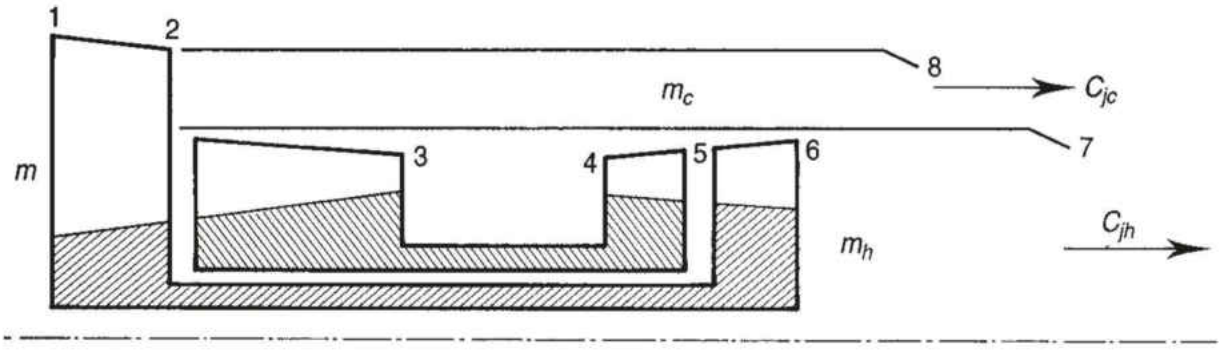

Figure 4. Conventional Turbofan Configuration [4]

Figure 4, at station 2 the cold stream exits the fan and travels through the fan chute and exhausts through the cold nozzle at station 8, whereas the hot stream is compressed through the stages of the compressor from station 1 to 3, is mixed with fuel and ignited in the combustion chamber from station 3 to 4, expanded through the stages of the turbine from station 4 to 6, and is then exhausted through the hot nozzle at station 7. While the bypass stream can provide thrust, the thrust produced by the bypass stream pales in comparison to the thrust produced by the core

stream [4]. Another unintended benefit of incorporating a bypass stream was that it significantly reduced noise production during operation [4]. This became especially important as commercial flights grew in demand and became increasingly popular and available [4]. Another type of turbofan that was developed is one where the hot and cold streams are mixed after the stages of the turbine, but prior to exhausting from a common nozzle. The mixing of the two streams proves to be advantageous in subsonic commercial aircraft as it reduces TSFC considerably while also increasing Fs [4]. In an effort to further augment thrust while also maintaining some of the benefits of the turbofan engine, scientists decided to implement an afterburner segment to low-bypass turbofan engines. This idea also addresses the issue of the lack of oxygen in the hot stream of a turbojet engine. With the mixing of the two streams, oxygen-rich air from the bypass stream is introduced into the core stream allowing for cleaner burning of the fuel in the afterburner segment. Figure 5 illustrates the configuration of a turbofan where the hot and cold streams mix in a constant-area duct.

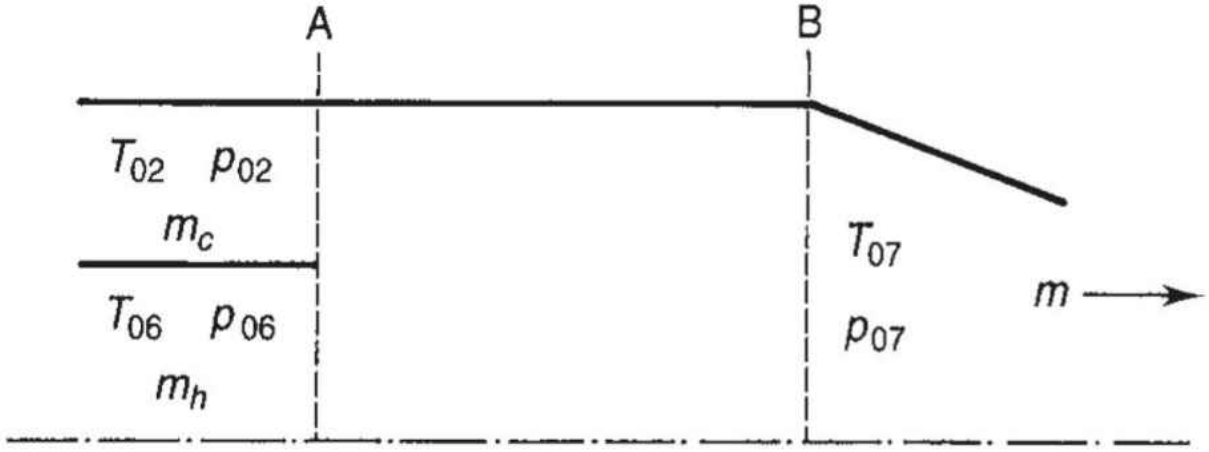

Figure 5. Constant-Area Mixing Duct [4]

Plane A in Figure 5 represents the entrance of the two separate streams into the duct and upon reaching plane B, the two streams will have completely mixed into one stream [4]. The modeling of this mixing occurring will be derived in detail in the formulation section.

New and Future Propulsion Systems and Technologies

As scientists and researchers continue to build upon current ideas and strive towards further optimizing current operational technologies, oftentimes many new ideas and technologies are conceived. This section aims to address a few of the new and future technologies that are being studied as viable options to improve efficiency, lower fuel consumption, and increase thrust. The afterburner segment that is added to some engines is often considered as a secondary combustion chamber, and while it does augment a significant amount of thrust to the engine, it comes to no surprise that this technology increases fuel consumption. The primary issue with afterburners is that they are grossly fuel inefficient and their use is now almost strictly applied to military aircraft. The text *Gas Turbine Propulsion Systems* by MacIsaac and Langton [7] discuss a few of the new possibilities and technological advancements that could pave a new future in aviation.

Over the last few decades, scientists have tirelessly dedicated their efforts to improving component efficiencies, and while this will undoubtedly increase thermal efficiency, the improvements that computational fluid dynamics have already contributed have developed this field exponentially and further improvement is becoming increasingly difficult to come across absent of proprietary breakthroughs and discoveries [7]. The two principle cycle design parameters for any gas turbine engine that improve efficiency are overall pressure ratio (OPR) and turbine inlet temperature (TINT) [4,7]. In recent decades, advancements in material science have made it possible to achieve higher TINTs and increase OPR [7]. Figure 6 below illustrates

the advancements in OPR achieved throughout history and it is interesting to note that with an OPR of 50:1, the stagnation temperature of ~960K entering the Rolls Royce Trent1000 combustion chamber is on par with the stagnation temperature exiting the combustion chamber of the first ever turbojet developed by Whittle in 1941 [7].

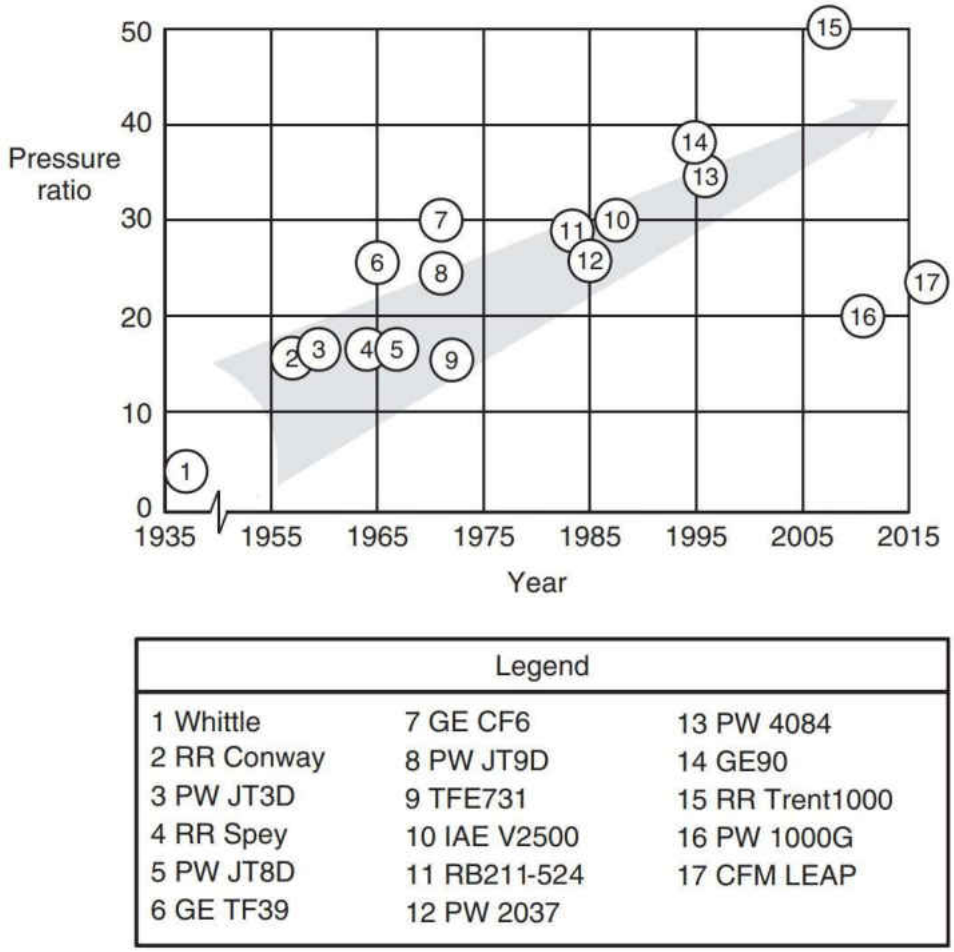

Figure 6. OPR Advancements Over Time [7]

As the world's leader in defense spending and military power, the US government has shown great interest in the advancement of technologies that improve cycle efficiency and has

funded work under the integrated high-performance turbine engine technology program (IHPTET) [7]. Some of the research conducted was devoted to the integration of high-temperature resistant materials such as ceramics [7]. Although they are exceptionally heat resistant, the issue with ceramics is their lack of ductility and their propensity to fail suddenly and catastrophically, so scientists have narrowed their efforts to ceramic composites as an effort to preserve the heat-resistant nature of ceramics while also incorporating the ductile nature of certain metals [7]. The technology has advanced to the point where it is being seriously considered in applications of non-rotating components such as nozzle vanes and liners [7]. The defense industry has demonstrated the successful application of ceramic composites in rotating turbine blades in military aircraft, but it may be years before these advancements are applied to commercial engines [7]. Another advantage of ceramic composites is the reduction in weight they provide [7]. The integration of ceramic composites in a turbine system suggests a weight reduction of 30% [7].

In August 2020, Kourosh Vaferi and his co-authors published their research on ultrahigh temperature ceramic composites (UHTC) as an alternative to superalloys in gas turbine stator blades to the Ceramic International journal [8]. In this journal publication, they discuss how the efficiency of the Bryton cycle relies heavily on the maximum temperature achievable [8]. Conventional turbines use superalloys such as M152 in the turbine blades, but Vaferi and his team analyzed the heat and stress distributions of SiC reinforced HfB_2 and ZrB_2 UGTCs using finite element analysis [8]. Vaferi and his team investigated the possible application of these ceramic composites in turbine stator blades due to the fact that there is no centrifugal force acting on stator blades thus tensile stresses can be ignored; meaning the main sources of generated stresses in turbine stator blades are thermal stresses and fluid flow forces [8]. With the absence

of centrifugal forces to cause tensile stresses, the thermal stresses in the stator blades are compressive in nature, and materials that are not only resistant to high temperatures, but also resistant to compressive stresses are required [8]. UHTCs satisfy these requirements. In their analysis of these materials, they investigated how temperature affected the thermal conductivity and coefficient of thermal expansion (CTE) in these proposed stator blades in an attempt to predict the deformation and thermal stresses that would occur [8]. This was achieved by solving the heat transfer and stress-strain equations numerically [8]. Below are the graphs of how the UHTCs and their properties were affected by temperature.

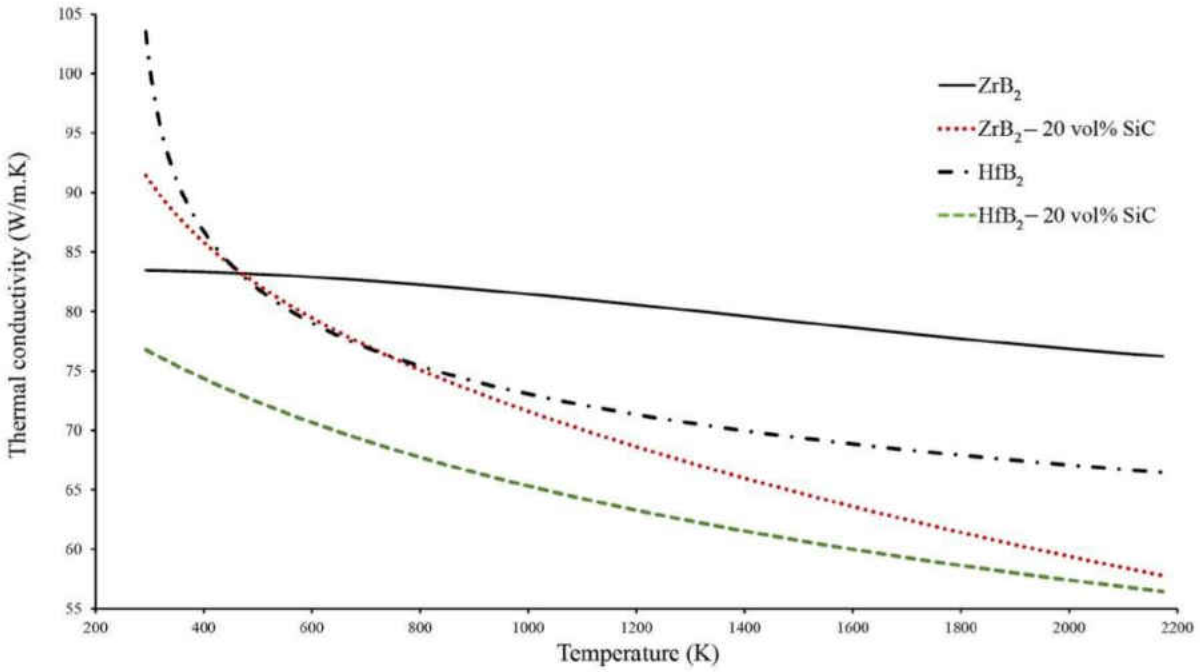

Figure 7. Thermal Conductivity vs. Temperature [8]

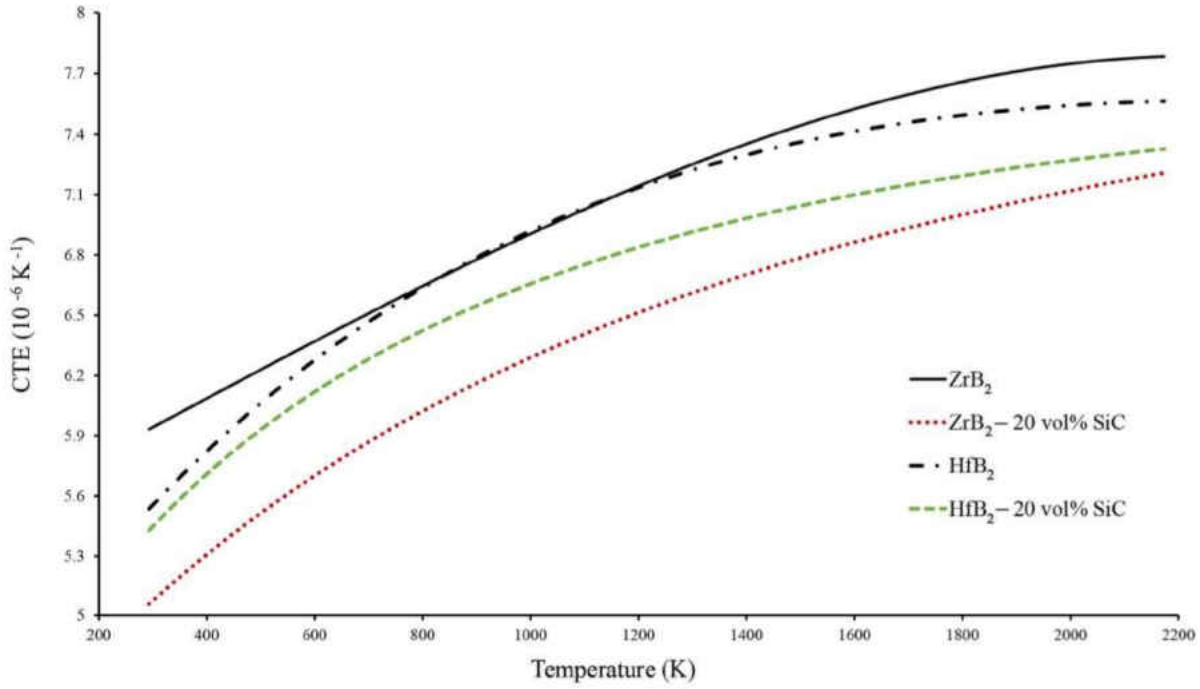

Figure 8. Coefficient of Thermal Expansion vs. Temperature [8]

Of the UHTCs studied, the ZrB_2–SiC composite material had a higher thermal conductivity in comparison with HfB_2–SiC [8]. A higher thermal conductivity translates to a more uniform and proper temperature distribution in the stator blade [8]. Similarly shown in the graph of the CTE as a function of temperature, ZrB_2–SiC exhibited a lower heat expansion coefficient which reduces the applied stresses and displacements in the blade [8]. Among the composites studied, ZrB_2–SiC presented the best case for its use in manufacturing of turbine stator blades due to its higher thermal conductivity, allowing for a more even thermal distribution, and its lower CTE, meaning less displacement [8].

As aforementioned, another means of seeking to further augment thrust while aiming to maintain fuel consumption and increase efficiency is the implementation of a second combustion chamber such as an inter-turbine burner (ITB) in a conventional, separate-exhaust turbofan

engine. This is done by placing a secondary combustion chamber between the low and high-pressure turbines [9,10,11]. Jakubowski's journal publication on a two-combustor turbofan engine studies the performance of an ITB in comparison with a conventional turbofan engine. Figure 9 illustrates the configuration of the proposed engine.

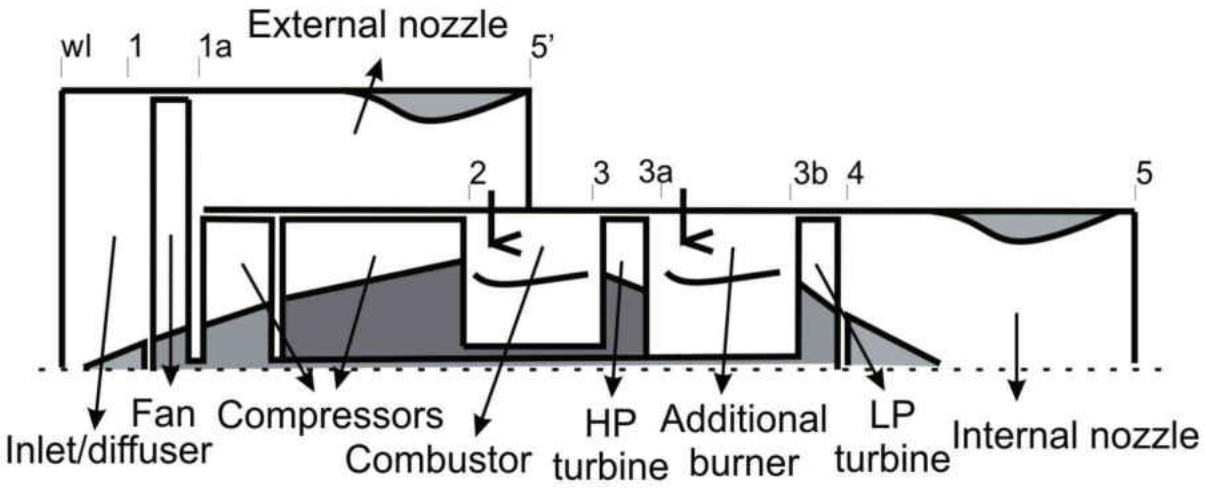

Figure 9. Commercial Turbofan with ITB [9]

From stations 1 to 3a, the configuration is identical to that of a conventional turbofan engine, but between stations 3a and 3b, the high-pressure and low-pressure turbines, there is an additional burner. Jakubowski explains that conventional turbofan engines have TINTs of 1700K+ and for the turbines to withstand such high temperatures, complex turbine blade cooling systems which extract a lot of air from the core stream thus lowering the thermal efficiency of the engine [9]. The conception of this design is primarily to allow for lower TINTs to 1300K while still producing thrust comparable to conventional turbofan engines [9]. When the TINT is lowered, these complex cooling systems are no longer necessary and allow for a simpler and cheaper design to manufacture and maintain [9]. Lower TINTs also mean that the turbine blades

are under significantly less stress and this allows for longer life cycles which will be beneficial from an economic standpoint [9]. In Liew's investigation of ITBs, he states that the fuel is burned at pressures higher than in an afterburner which results in higher thermal efficiency and that the major benefits associated with incorporating an ITB are increasing thrust and reducing environmentally harmful NO_x emissions [10]. Both Jakubowski and Liew also studied the effects of design parameters, such as flight speed and altitude, on engine performance and the graphs below illustrate Jakubowski's findings.

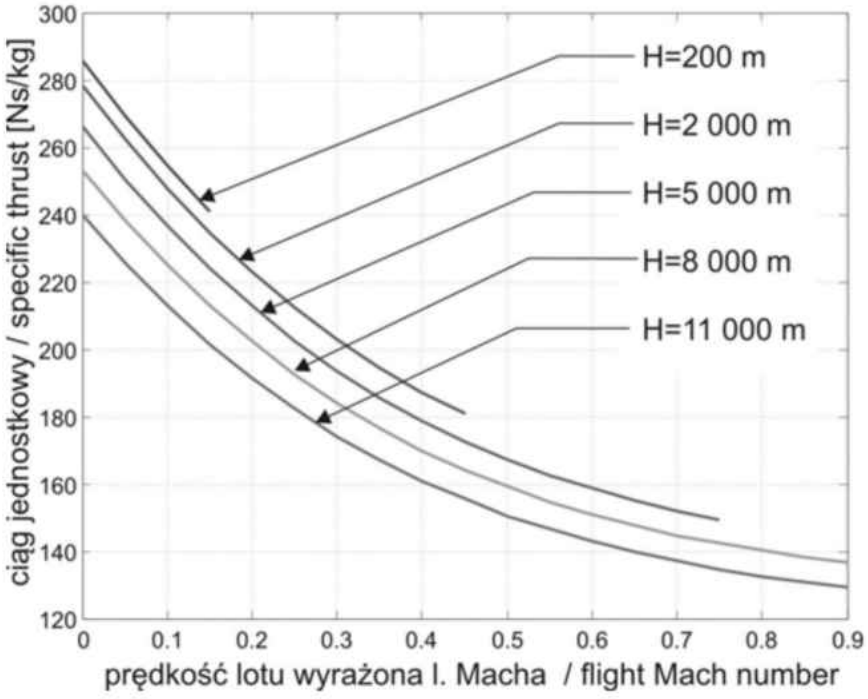

Figure 10. Fs vs. Flight Speed [9]

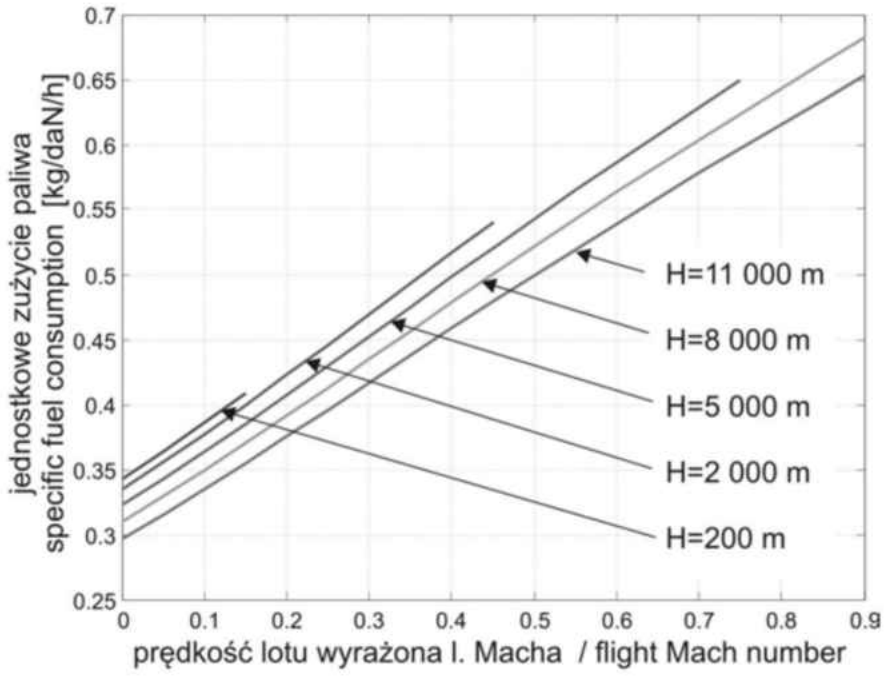

Figure 11. TSFC vs. Flight Speed [9]

Both authors conclude that the use of ITBs in aircraft seem promising with Jakubowski noting that the two-combustor engine in his study required a smaller OPR to produce the same amount of thrust as a conventional turbofan engine while mass flow is constant [9,10]. While a smaller OPR does increase TSFC under take-off conditions, the two-combustor engine exhibited a lower TSFC during cruise conditions in the Mach 0.8 range that commercial airlines fly at [9]. Liew confirmed this finding stating that the "ITB engine at full throttle setting has enhanced performance over baseline engine… ITB operating at partial throttle will exhibit high thrust at lower S (specific fuel consumption) and improved thermal efficiency over the baseline engine [10]."

The idea of implementing secondary proves promising and while the idea of a secondary burner in gas turbine engines is not a novel one, Asundi and his colleagues proposed implementing an auxiliary combustion chamber not in between the turbine stages, but in the fan

chute of a turbofan engine. Their journal publication discusses the motivations for their research as a means of facilitating clean secondary burning of fuel at higher temperatures than currently achievable [5]. They also mention that advancements in materials science for high-temperature applications, such as ceramic composites, shows a promising future for the application of their auxiliary burner in operational engines [5]. Their novel proposed engine is not too dissimilar to a conventional turbofan engine. Their configuration consists of three streams: a core stream, a low-pressure bypass stream (LPB), and a high-pressure bypass stream (HPB) or auxiliary high-pressure bypass stream (AHBP) [5]. The configuration of this engine is illustrated in the figure below.

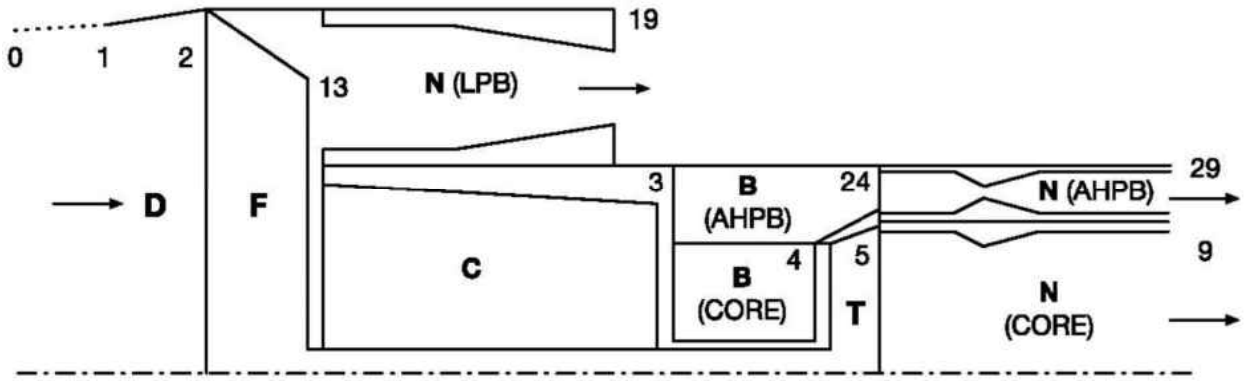

Figure 12. Turbofan with an Auxiliary High-Pressure Bypass Configuration [5]

Stations 1 to 3 and 1 to 19 are identical to that of a conventional turbofan engine, but the core stream, upon exiting the high-pressure compressor at station 3, diverges into two streams. The core stream enters the main combustion chamber, enters the turbine, then exhausts from the core nozzle. The AHPB stream enters station 24, the AHPB combustion chamber, and is combusted at 2516K. These high temperatures are achievable since the AHPB does not enter the turbine where it would cause catastrophic damage. Instead, the AHPB exhausts from a separate

nozzle. With this configuration, they investigated the performance of the engine with respect to thrust output, fuel consumption, and efficiency as the LPB and AHPB ratios varied [5]. The benefit of this configuration as opposed to an afterburning engine or an ITB engine is that the combustion that occurs in the AHPB combustion chamber is carried out using air which is not previously depleted of its oxygen and at higher stagnation pressures than an afterburner or ITB thus increasing the engine efficiency while simultaneously minimizing fuel consumption penalties. Their findings were that as LPB ratio decreased and AHPB ratio increased, Fs and TSFC both increased, but they state that the increase in TSFC can likely be attributed to the decrease in the LPB ratio [5].Their parametric analysis was modeled with the use of computer programs and it is worthy to note that the assumptions made were of isentropic flows throughout the engine [5]. They conclude by saying that their results were promising but further analysis is required under non-isentropic conditions and assumptions in hopes of arriving at results that would make a strong case for its application in certain aircraft [5]. As a continuation of their work, the TurboAux is an attempt to improve upon their design and will be presented in the coming chapters along with a detailed formulation on the thermodynamics therein.

Statement of Work and Objectives

Expanding on the ideas and the research of Asundi and Ali, the objective of this research is to investigate the performance of turbojet and turbofan engines (as well as their afterburning counterparts) and identify their positive and negative characteristics. Then it is necessary to analyze the performance and characteristics of the TurboAux. The next step is to compare the three engines to each other in hopes of finding a useful and viable application for the TurboAux. Finally, the TurboAux will be presented in comparison to current and former operational engines

to serve as a litmus test for its usefulness for a wide range of applications. The analysis of these engines is done with the use of a computer program, MATLAB, to accurately model the thermodynamics under realistic parameters and component efficiencies. This analysis was conducted on a per-unit-mass-flow basis meaning that some of the parameters, aside from stagnation temperature, pressure, and other such flow properties, are calculated as specific quantities (for example the specific work required to run the compressors and the specific thrust output of the engine). Conducting this analysis this way allows for one to compare these results to any engine of similar configuration and will be presented in a trade study in a later chapter.

CHAPTER II

OPTIMIZATION ANALYSIS

In this chapter, the results and the findings of the optimization analysis are presented. The performance of a low-bypass turbofan was analyzed in an attempt to find an optimum engine configuration that would be used to model the TurboAux engine. The turbojet has two thermodynamic properties that can be varied to study its changes in performance: OPR and TINT, while the turbofan engine has four thermodynamic properties which can be manipulated to study engine performance: OPR, TINT, bypass ratio (BPR), and fan pressure ratio (FPR) [4]. When studying these engines, OPR and TINT were fixed while FPR and BPR were varied to see their effects on various performance parameters. Full mathematical formulation will be presented in the next chapter.

Prior to conducting the optimization analysis of the low-bypass turbofan engine, the difference in performance between a turbojet engine and a conventional turbofan engine (where the two streams do not mix) was investigated. All engine comparisons were conducted under the same parameters and flight conditions which can be shown in the table below. An altitude of 5km was selected and the corresponding ambient conditions were adopted from International Standard Atmosphere standards. Most close-air-support aircraft fly around that range thus the reason for its selection. Future analysis will be conducted at higher altitudes ~10km to compare to higher performance military aircraft. Table 1 below presents the design points for all of the engines in this parametric analysis

Table 1. Design Points

Flight Conditions:	$M_a = 0.84$	$P_a = 54.05$ kPa	$T_a = 255.7$ K
Air Properties:	$C_{p0air} = 1004.5$ J/kg·K	$\gamma_{air} = 1.4$	$R_{air} = 287$ J/kg·K
Gas Properties:	$C_{p0gas} = 1148$ J/kg·K	$\gamma_{gas} = 1.3333$	$R_{gas} = 287$ J/kg·K
Other Parameters:	TINT = $T_{04} = 1922$ K	$T_{aux} = T_{08} = 2516$ K	$\pi_c = 50$
Efficiencies	$\eta_d = 0.93$	$\eta_c = 0.93$	$\eta_b = 0.98$
	$\eta_m = 0.99$	$\eta_t = 0.90$	$\eta_n = 0.95$
Fuel Properties:	$H_{rpf} = -8561991.6$ kJ/kmol	$M_{fuel} = 197.7$ kmol/kg	HV = 43308000 J/kg
	Moles of Carbon (MC) = 14.4	Moles of Hydrogen (MH) = 24.9	Moles of Oxygen (MO) = 0
Other Properties:	$H_{rpCO2} = 282800$ kJ/kmol	$M_{air} = 28.97$ kmol/kg	

Using the same fuel properties and flight conditions as well as component efficiencies adopted from *Gas Turbine Theory* [4], the effect of a varying FPR (while holding the bypass ratio for the turbofan at 1.5) on Fs and TSFC was studied. The results showed the turbojet engine produced a significant amount more Fs than the conventional turbofan engine but the turbofan engine's TSFC was less than that of the turbojet engine. The FPR values were varied from 1.3 to 7 and the turbojet and turbofan showed contrasting trends for Fs. As FPR increased, Fs values for the turbojet decreased, but for the turbofan the Fs values increased across this same range. In both engines however, TSFC decreased as FPR increased. These trends are illustrated in the figures 13 and 14.

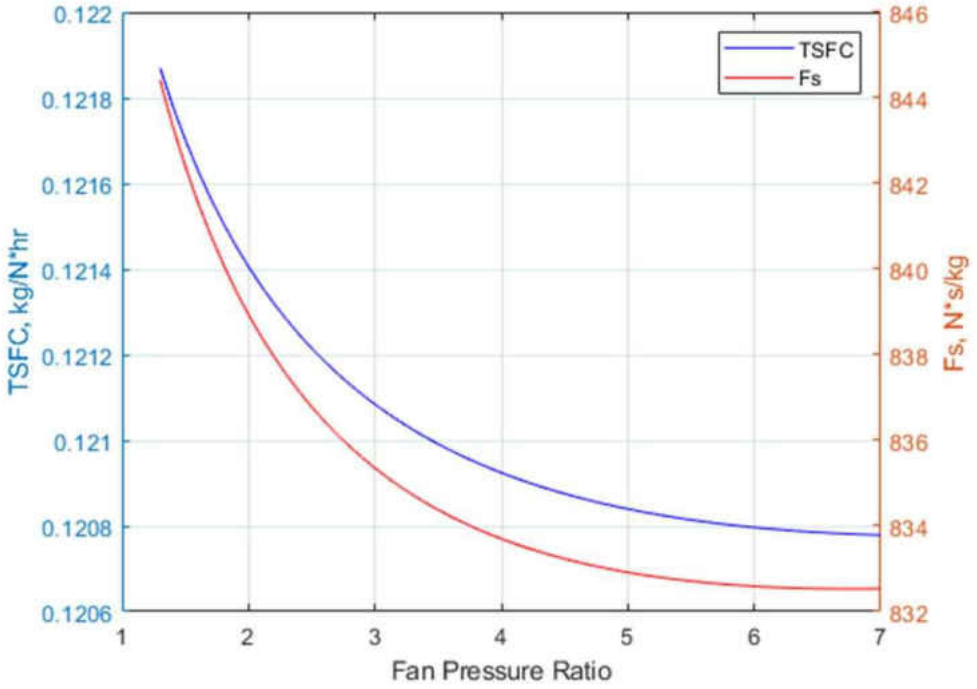

Figure 13. Turbojet Performance vs. FPR

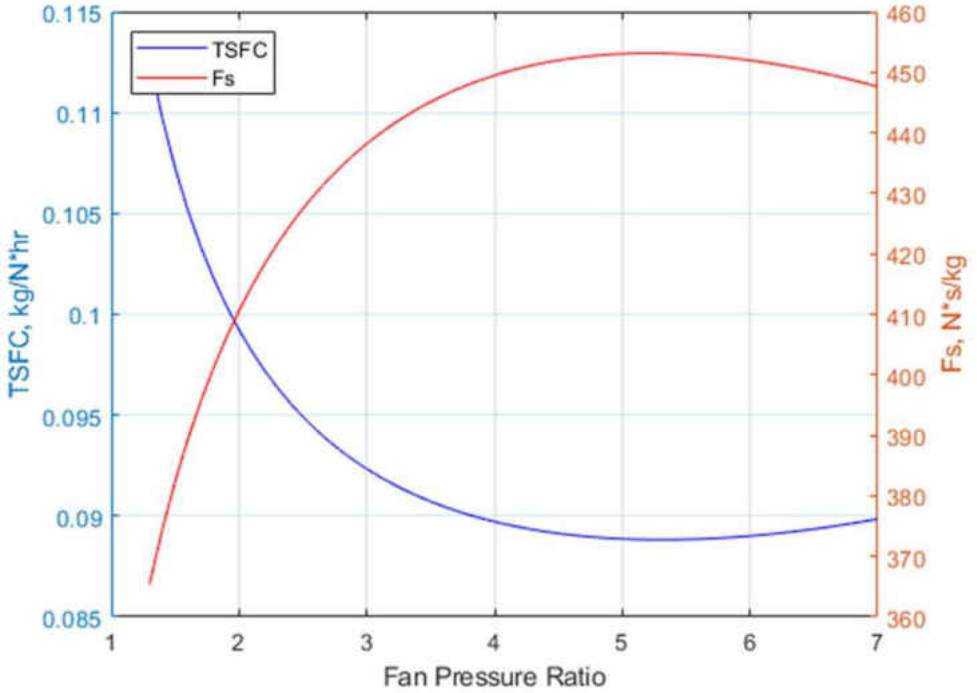

Figure 14. Turbofan Performance vs. FPR

It that was evident from the analysis was that as the BPR decreased in the turbofan configuration, Fs and TSFC increased and the turbofan exhibited increasingly similar trends to that of the turbojet. This served as first-hand evidence as to why low-bypass turbofans are used in military aircraft applications as they perform similarly while still improving on some of the issues with turbojet engines.

The next step in this analysis was to investigate the differences between two similar turbofans: the conventional turbofan where the two streams exhaust separately and the military-style turbofan where the two streams mix and exhaust from one nozzle. Again, both configurations were studied with the same design points, component efficiencies, ambient conditions, and fuel characteristics. For every BPR investigated, ranging from 0.1 to 1.5, the military-style turbofan outperformed the conventional turbofan with respect to both Fs and TSFC as well as a few other performance parameters. Tables 2-4 below show some of the comparisons in their performance. The performance of the turbojet has also been included as comparison in Tables 2-4 as a reference to show how bypass ratio affects the conventional and military-style turbofan engines.

Table 2. Performance with Bypass Ratio Fixed at 0.1

Engine	Fs	TSFC	Propulsive Efficiency	Thermal Efficiency	Overall Efficiency
Conventional Turbofan	771.8685349	0.121203965	60.54%	30.50%	18.47%
Military-style Turbofan	800.8456980	0.116818417	62.47%	30.67%	19.16%
Turbojet	844.4112539	0.121870568	60.29%	30.46%	18.36%

Table 3. Performance with Bypass Ratio Fixed at 0.5

Engine	Fs	TSFC	Propulsive Efficiency	Thermal Efficiency	Overall Efficiency
Conventional Turbofan	616.8973001	0.109334222	67.38%	30.38%	20.47%
Military-style Turbofan	658.3954498	0.102442972	71.16%	30.70%	21.85%
Turbojet	835.4729081	0.121095464	60.75%	30.42%	18.48%

Table 4. Performance with Bypass Ratio Fixed at 1.5

Engine	Fs	TSFC	Propulsive Efficiency	Thermal Efficiency	Overall Efficiency
Conventional Turbofan	447.2147327	0.089936632	87.97%	28.29%	24.89%
Military-style Turbofan	507.3070444	0.079283320	83.25%	33.91%	28.23%
Turbojet	832.5385947	0.120778145	60.90%	30.43%	18.53%

These simulation results provide justification to the selection of the low-bypass, military-style turbofan as the base configuration being optimized and later adapted with an auxiliary combustion chamber in the bypass stream. As illustrated in the Tables 2-4, the military-style turbofan outperformed the conventional turbofan in all parameters and outperformed the turbojet in all except Fs. The optimization process is an attempt to close this gap between the two engines.

Optimizing the Low-Bypass Turbofan

When optimizing the turbofan, there are four thermodynamic parameters that can be manipulated to investigate their effects on performance [4]. As aforementioned these parameters are OPR, TINT, FPR, and BPR. The OPR and TINT are thought to determine the "quality" of the engine cycle, while FPR and BPR characterize the effectiveness with which the available energy is converted to thrust [4].

For a given BPR, as FPR is increased, the thrust produced by the bypass stream will increase but this requires more and more energy to be extracted from the core stream thus decreasing the core stream thrust output [4]. Conversely, for low values of FPR at a fixed BPR, the thrust produced by the core stream will be high and little energy will be extracted from the core stream to drive the fan [4]. If OPR and BPR are fixed and a value for TINT is selected, then the energy input for the engine is fixed since the combustion chamber air flow and entry temperature are determined by those operating conditions [4]. This means that the optimum FPR values for maximizing Fs and minimizing TSFC coincide. From this understanding, when analyzing the low-bypass turbofan, OPR was fixed at 50 and TINT was fixed at 1922K. Then, a BPR of 0.1 was selected as FPR varied from 1.3 to 7 to find the optimal configuration. This cycle was repeated for several BPRs ranging from 0.1 to 1.5 and yielded a set optimal designs; designs in which with OPR and TINT fixed, every BPR had a coinciding FPR that maximized Fs and minimized TSFC simultaneously. This optimization was first done for a low-bypass turbofan with two separate streams exhausting from separate nozzles and from previous understanding, it seemed a reasonable assumption that this optimal configuration would hold true as well for a military-style low-bypass turbofan with mixing of the hot and cold streams, as mixing only

further improved the performance of the engine with respect to Fs, TSFC, and engine efficiency. The optimal FPR value found for each BPR is tabulated in Table 5.

Table 5. Optimal FPR Values

Bypass Ratio	Optimum FPR (for min TSFC)	TSFC (kg/N·hr)	Optimum FPR (for max Fs)	Fs (N·s/kg)
0.1	7	0.1171728397	7	780.1416178
0.2	7	0.1138469486	7	736.0214069
0.3	7	0.1107785118	7	698.223092
0.4	7	0.107948488	7	665.3474361
0.5	7	0.1053409233	7	636.3626873
0.6	7	0.1029426509	7	610.4888783
0.7	7	0.1007430776	7	587.1228077
0.8	7	0.09873405261	7	565.787852
0.9	7	0.09690981607	7	546.0994217
1.0	7	0.09526703122	7	527.740543
1.1	6.7	0.09378563802	6.6	510.5675219
1.2	6.2	0.09241252053	6.2	494.6515586
1.3	5.9	0.09113389451	5.8	479.8541449
1.4	5.6	0.08994122323	5.5	466.0477838
1.5	5.3	0.08882537546	5.2	453.1261646

It is interesting to note that from a BPR of 1 to 1.5, some of the optimum FPR values for maximizing Fs and minimizing TSFC do not exactly coincide. The reason for this still requires further investigation but the discrepancies in the optimum values are minuscule and as an effort

to minimize fuel consumption, the optimum FPR values that minimized TSFC were selected for the final optimal design. Lee in his investigation of two-combustor engines also found that the optimal FPR for maximizing Fs and minimizing TSFC did not coincide, noting that the optimum FPR for maximizing Fs was less than the optimum FPR for minimizing TSFC [11]. Figures 15-20 are some of the graphical representations of the effects of FPR on Fs and TSFC while OPR and TINT are fixed for a chosen BPR. It can be noted that as bypass ratio increases, the curves for Fs and TSFC transition from trending linearly to trending logarithmic and parabolically, making the optimal points increasingly easy to identify graphically.

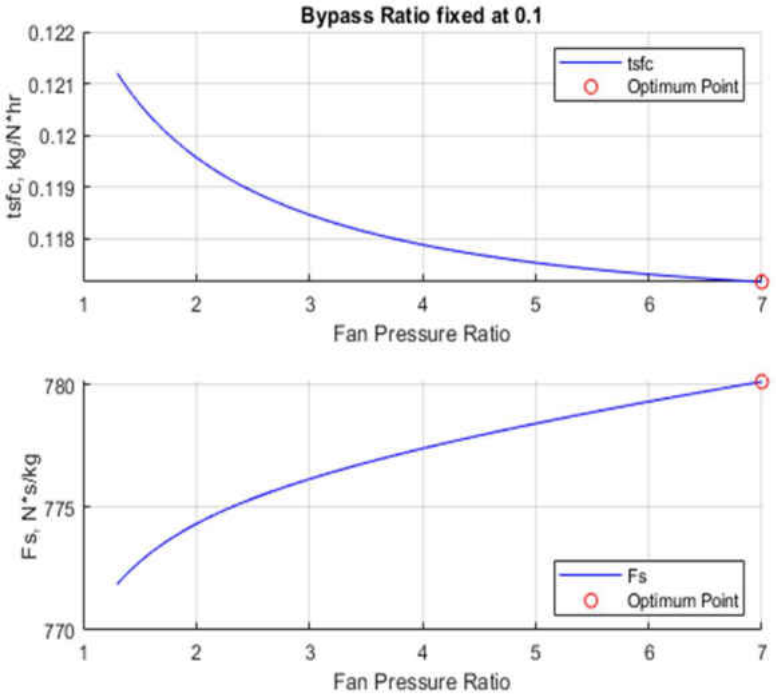

Figure 15. Optimum FPR with BPR at 0.1

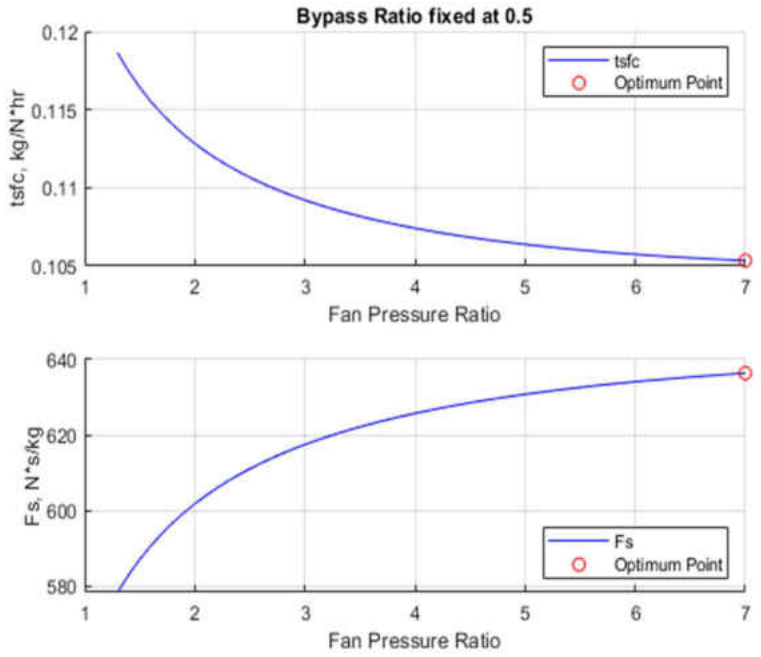

Figure 16. Optimum FPR with BPR at 0.5

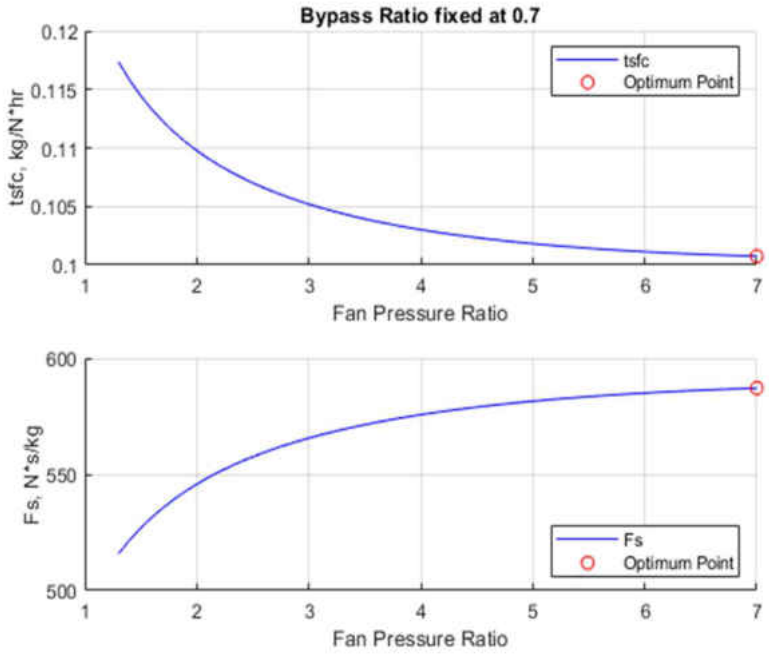

Figure 17. Optimum FPR with BPR at 0.7

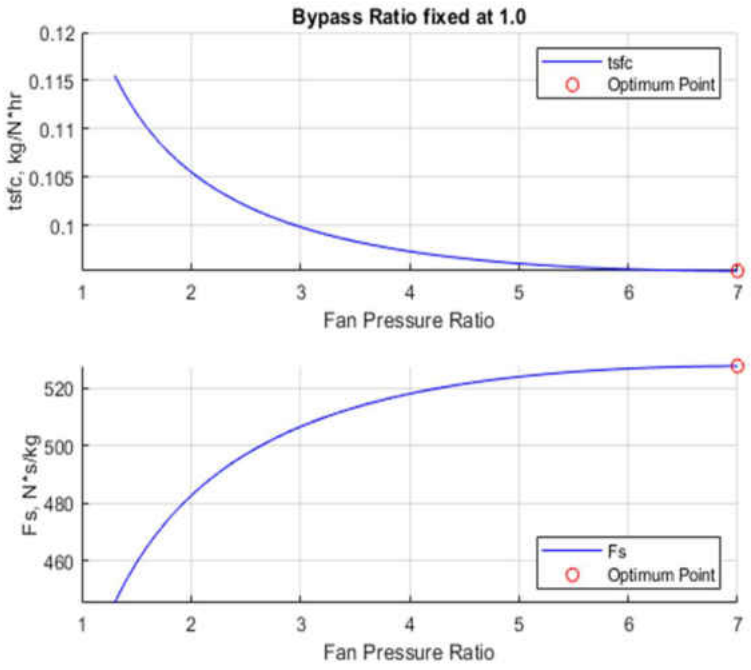

Figure 18. Optimum FPR with BPR at 1.0

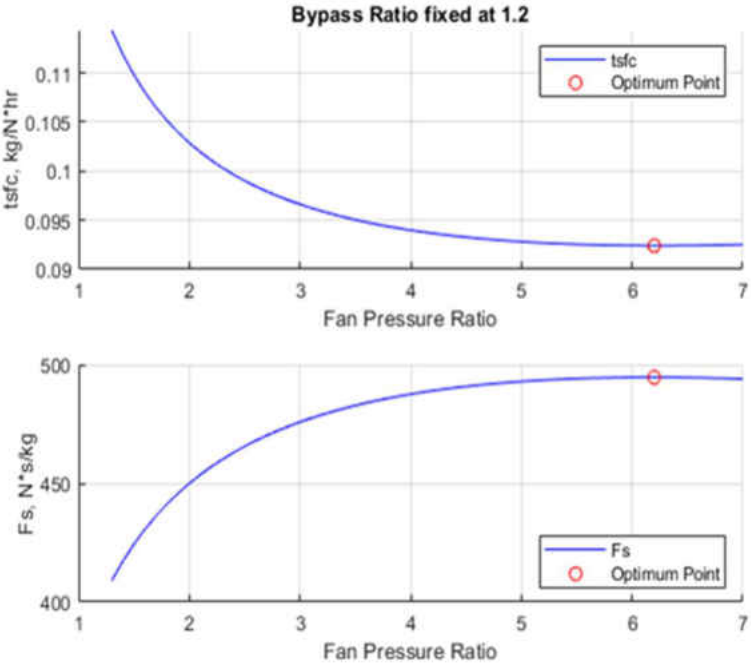

Figure 19. Optimum FPR with BPR at 1.2

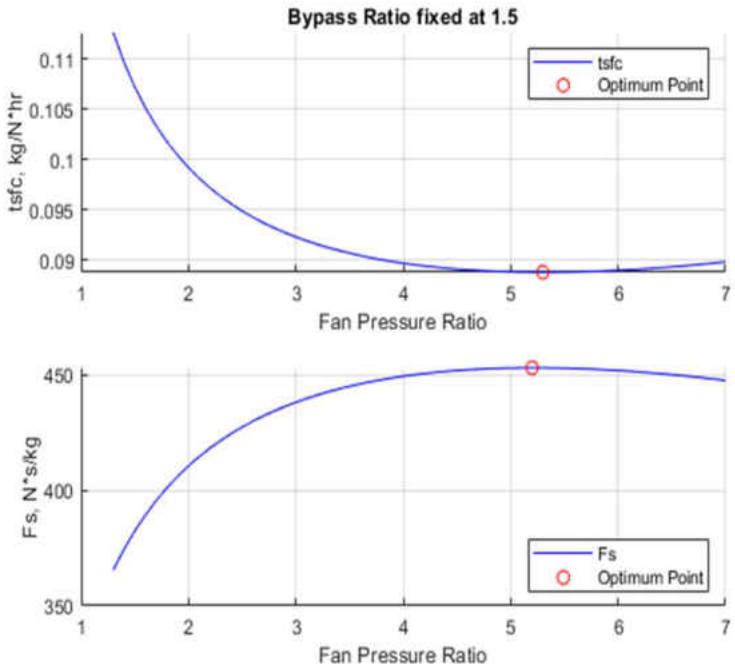

Figure 20. Optimum FPR with BPR at 1.5

CHAPTER III

MATHEMATICAL FORMULATION OF THE TURBOAUX, TURBOJET, AND TURBOFAN

This chapter is a presentation of the mathematical formulation, calculation, and derivation for the TurboAux, turbojet, and turbofan engines studied in MATLAB to arrive at the results presented in the next chapter. The engines that are presented in this chapter are the TurboAux, the turbojet with an afterburner segment, and the military-style turbofan with an afterburner segment. Flight conditions and other simulation parameters and properties were selected to coincide with current flight conditions of similar engines and are summarized in Table 1. When modeling the thermodynamics of these engines, a few assumptions were made:

- All component efficiencies and specific heat capacities are constant.
- Combustion chambers are adiabatic but account for frictional losses.
- The streams will mix fully in the constant-area mixing duct.
- The is no dissociation occurring in the products of combustion.

TurboAux Configuration and Formulation

The TurboAux engine is an extension of the military-style low-bypass turbofan. The configuration of the TurboAux is almost identical to that of the military-style low-bypass turbofan apart from the auxiliary combustion chamber augmented into the bypass stream which is illustrated in Figure 21 from stations 2 to 8. The two streams will mix at station 7 and exhaust from a common nozzle at station 9. Below is the configuration of the conceived TurboAux engine.

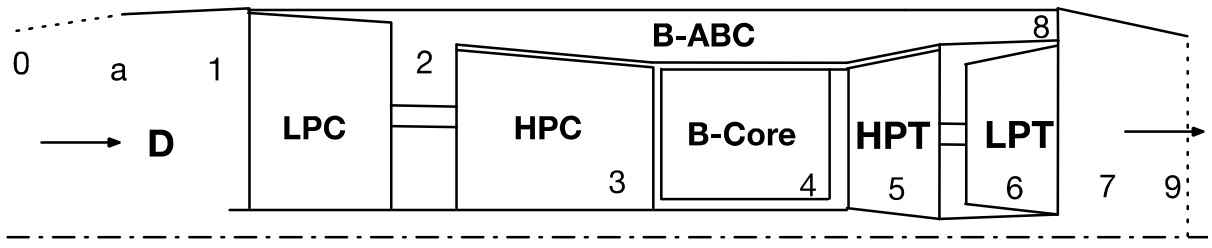

Figure 21. Conceptual Design Configuration of the TurboAux Engine

After optimizing the low-bypass turbofan as presented in the previous chapter, the optimized design obtained from the analysis will be adopted for all the models to serve as comparison to the TurboAux. It is important to note that these engines are of similar design thus sharing many equations. To avoid redundancy, presented below is the formulation for the TurboAux and the subsequent sections will present the equations used to model the other engines.

The local speed of sound and the flow speed at the inlet of the of the diffuser are computed in equations (1) and (2), respectively. Upon entering the diffuser, the stream is slowed down and the new stagnation temperature and pressure of the stream due to the reduction in velocity and diffuser efficiency are calculated in equations (3) and (4), respectively.

$$C = \sqrt{\gamma_a \cdot R_a \cdot T_a} \tag{1}$$

$$V_a = M_a \cdot C \tag{2}$$

$$T_{01} = T_a \left[1 + \left(\frac{\gamma_a - 1}{2} \cdot M_a^2\right)\right] \tag{3}$$

$$P_{01} = P_a \left[1 + \eta_d \cdot \left(\frac{\gamma_a - 1}{2}\right) \cdot M_a^2\right]^{\frac{\gamma_a}{\gamma_a - 1}} \tag{4}$$

After the diffuser, the flow is compressed by the low-pressure compressor (LPC) or "fan". The stagnation pressure is simply found as the product of the pressure ratio across the fan (FPR). The optimum FPR values from the optimized design are used here in equation (5). The stagnation temperature is computed in equation (6) which accounts for the efficiency of the compressor and the specific work required to operate the LPC is computed in equation (7).

$$P_{02} = P_{01} \cdot \pi_{LP} \tag{5}$$

$$T_{02} = T_{01} + \left\{ \frac{T_{01}\left[\left(\pi_{LP}^{\frac{\gamma a-1}{\gamma a}}\right)-1\right]}{\eta_c} \right\} \tag{6}$$

$$W_C^{LP} = (B+1) \cdot C_{p0a} \cdot (T_{01} - T_{02}) \tag{7}$$

Following the compression of the stream in the LPC, the stream diverges into two streams: the core stream and the auxiliary stream. The bypass ratio is defined in equation (8). The auxiliary stream bypasses the core of the engine and enters the auxiliary combustion chamber, while the core stream is compressed further through the stages of the high-pressure compressor (HPC). The combustion process of the auxiliary combustion chamber will produce products of combustion at 2516 K. The loss in stagnation pressure in this combustion process is calculated in equation (9).

$$B = \frac{\dot{m}_{aux}}{\dot{m}_{core}} \tag{8}$$

$$P_{08} = P_{02} \cdot (\eta_b) \tag{9}$$

The compression ratio of the HPC is calculated in equation (10) as the overall pressure ratio divided by the FPR. The stagnation pressure, stagnation temperature, and specific work

required to operate the HPC are computed in similar manner as in the LPC in equations (11), (12), and (13) respectively.

$$\pi_{HP} = \frac{\pi_C}{\pi_{LP}} \tag{10}$$

$$P_{03} = P_{02} \cdot \pi_{HP} \tag{11}$$

$$T_{03} = T_{02} + \left\{ \frac{T_{02}\left[\left(\pi_{HP}^{\frac{\gamma a-1}{\gamma a}}\right)-1\right]}{\eta_c} \right\} \tag{12}$$

$$W_C^{HP} = C_{p0a} \cdot (T_{02} - T_{03}) \tag{13}$$

The combustion process is assumed as a complete combustion process with excess air in the products and was modeled in both the auxiliary and main combustion chambers using the enthalpy of reactions, enthalpy of combustion, and the first law of thermodynamics. Equations (14) and (15) are equations used calculate the specific enthalpy, on a molar basis, of each constituent in the combustion process. The constants a, b, and c are experimental coefficients taken from literature used in the calculation of the specific enthalpy [12]. Equation (16) calculates the change in the specific enthalpy. Due to temperature limitations of the turbine blades, the products of combustion from the main combustion chamber are exiting at 1922 K. The number of moles for stoichiometric combustion of the fuel is computed in equation (17), and with the fuel, temperature of the reactants, and the temperature of the products specified, the number of moles of air required for complete combustion with excess air in the products is calculated in equation (18).

$$\bar{h}_{Tr} = a + b \cdot Tr + c \cdot ln(Tr) \tag{14}$$

$$\bar{h}_{Tp} = a + b \cdot Tp + c \cdot ln(Tp) \tag{15}$$

$$\Delta\bar{h} = \bar{h}_{Tp} - \bar{h}_{Tr} \tag{16}$$

$$Y_{cc} = MC + \left(\frac{MH}{4}\right) - \left(\frac{MO}{2}\right) \tag{17}$$

$$y = \frac{-Hrp_f - (MC)\Delta\bar{h}_{CO_2} - \left(\frac{MH}{2}\right)\Delta\bar{h}_{H_2O} + (Y_{cc})\Delta\bar{h}_{O_2}}{(3.76)\Delta\bar{h}_{N_2} + \Delta\bar{h}_{O_2}} \tag{18}$$

After the number of moles of air required for complete combustion is calculated in equation (18), equation (19) computes the ideal fuel to air ratio on a mass basis. To account for non-ideal combustion, the actual fuel to air ratios for both the main combustion chamber and the auxiliary combustion chamber are computed in equations (20) and (21) respectfully. Losses in stagnation pressure due to friction and combustion are calculated in equation (22). Conservation of mass states that the total mass flow rate of fuel is the sum of the separate mass flow rates in equation (23). Using the bypass ratio, the overall fuel to air ratio of the entire engine accounting for both combustion processes is calculated in equation (24).

$$f_{ideal} = \left(\frac{1}{4.76 \cdot y}\right)\left(\frac{M_{fuel}}{M_{air}}\right) \tag{19}$$

$$f_{actual} = \frac{f_{ideal}}{\eta_b} = \frac{\dot{m}_{f1}}{\dot{m}_{core}} \tag{20}$$

$$f_{aux} = \frac{f_{ideal}}{\eta_b} = \frac{\dot{m}_{f2}}{\dot{m}_{aux}} \tag{21}$$

$$P_{04} = P_{03} \cdot (\eta_b) \tag{22}$$

$$\dot{m}_{ftot} = \dot{m}_{f1} + \dot{m}_{f2} \tag{23}$$

$$f_o = \left(\frac{B \cdot f_{aux}}{B+1}\right)\left(\frac{f_{actual}}{B+1}\right) = \frac{\dot{m}_{ftot}}{\dot{m}_{core}} \tag{24}$$

Upon exiting the main combustion chamber, the core stream will be expanded through the high-pressure turbine and the low-pressure turbine. Equations (25) and (26) calculate the stagnation temperature and pressure exiting the high-pressure turbine and entering the low-pressure turbine. Similarly, equations (27) and (28) calculate the stagnation temperature and pressure exiting the low-pressure turbine. Losses which occur due to the mechanical and component efficiency of the turbine are accounted for in these equations as well.

$$T_{05} = T_{04} + \left[\frac{W_C^{HP}}{\eta_m(1+f_{actual})\cdot C_{pog}}\right] \tag{25}$$

$$P_{05} = P_{04}\left\{1 - \left[\frac{1-\left(\frac{T_{05}}{T_{04}}\right)}{\eta_t}\right]\right\}^{\frac{\gamma_g}{\gamma_g - 1}} \tag{26}$$

$$T_{06} = T_{05} + \left[\frac{W_C^{LP}}{\eta_m(1+f_{actual})\cdot C_{pog}}\right] \tag{27}$$

$$P_{06} = P_{05}\left\{1 - \left[\frac{1-\left(\frac{T_{06}}{T_{05}}\right)}{\eta_t}\right]\right\}^{\frac{\gamma_g}{\gamma_g - 1}} \tag{28}$$

After the stages of the turbine, the core stream and the auxiliary stream will reunite and mix prior to exhausting through the nozzle. Figure 22 illustrates this configuration with the proper station numbers.

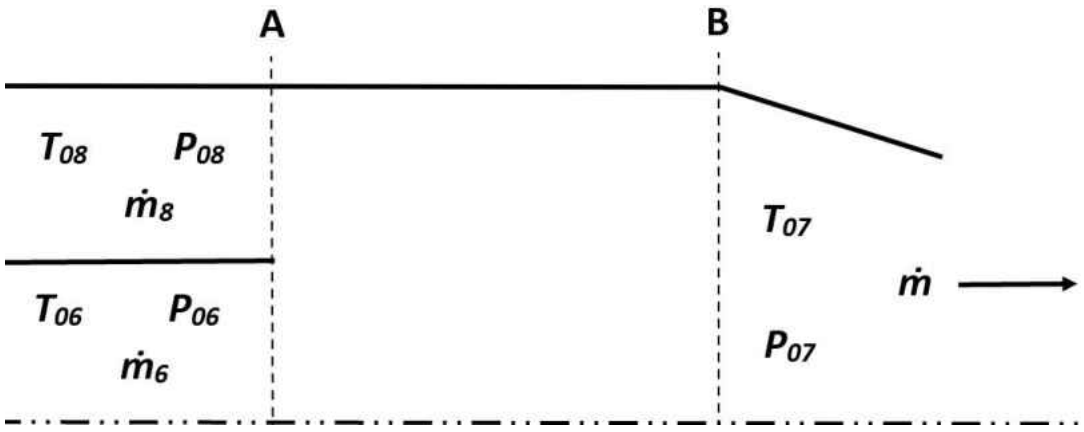

Figure 22. TurboAux Constant-Area Mixing Duct

In equation (43), the stagnation temperature of the mixed streams in calculated by manipulating conservation of energy, conservation of mass, and the first law of thermodynamics. Similarly, in equation (51), the stagnation pressure is a mass-weighted average of the two streams mixing. The derivation for those equations is as follows:

The conservation of energy balance is shown in equation (29) and conservation of mass in equation (30), states that the mass flow at plane B is the sum of the individual mass flow rates at plane A, and the individual mass flow rates are defined in equations (31) and (32).

$$\dot{m}_8 h_{08} + \dot{m}_6 h_{06} = \dot{m}_7 h_{07} \tag{29}$$

$$\dot{m}_8 + \dot{m}_6 = \dot{m}_7 \tag{30}$$

$$\dot{m}_6 = \dot{m}_{core} + \dot{m}_{f1} \tag{31}$$

$$\dot{m}_8 = \dot{m}_{aux} + \dot{m}_{f2} \tag{32}$$

Taking equations (30) and (31) and factoring out their respective air mass flow rates yields equations (33) and (34). Substituting equation (30) into equation (29) yields equation (35) and after subtracting the right-hand side over and simplifying, equation (36) is the result.

$$\dot{m}_6 = \dot{m}_{core}(1 + f_{actual}) \tag{33}$$

$$\dot{m}_8 = \dot{m}_{aux}(1 + f_{aux}) \tag{34}$$

$$\dot{m}_8 h_{08} + \dot{m}_6 h_{06} = (\dot{m}_8 + \dot{m}_6) h_{07} \tag{35}$$

$$\dot{m}_8 (h_{08} - h_{07}) + \dot{m}_6 (h_{06} - h_{07}) = 0 \tag{36}$$

Next, substitute equations (33) and (34) into equation (36) to get equation (37). Then, divide (37) by the mass flow of the core stream to yield equation (38). After substituting the stagnation enthalpies with the specific heat capacity at constant pressure of the gaseous mixture into equation (38), divide out C_{p0g} from (39) and distribute to arrive at equation (40).

$$[\dot{m}_{aux}(1 + f_{aux})(h_{08} - h_{07})] + [\dot{m}_{core}(1 + f_{actual})(h_{06} - h_{07})] = 0 \tag{37}$$

$$[B(1 + f_{aux})(h_{08} - h_{07})] + [(1 + f_{actual})(h_{06} - h_{07})] = 0 \tag{38}$$

$$\left[B(1 + f_{aux})C_{p0g}(T_{08} - T_{07})\right] + [(1 + f_{actual})C_{p0g}(T_{06} - T_{07})] = 0 \tag{39}$$

$$B(1 + f_{aux})T_{08} - B(1 + f_{aux})T_{07} + (1 + f_{actual})T_{06} - (1 + f_{actual})T_{07} = 0 \tag{40}$$

The last few steps are to isolate T_{07} to one side, factor out T_{07}, then divide everything else over to yield equations (41), (42), and (43) respectively.

$$B(1 + f_{aux})T_{07} + (1 + f_{actual})T_{07} = B(1 + f_{aux})T_{08} + (1 + f_{actual})T_{06} \tag{41}$$

$$T_{07}[(1+f_{actual})+B(1+f_{aux})] = B(1+f_{aux})T_{08}+(1+f_{actual})T_{06} \quad (42)$$

$$T_{07} = \frac{B(1+f_{aux})T_{08}+(1+f_{actual})T_{06}}{B(1+f_{aux})+(1+f_{actual})} \quad (43)$$

The derivation of P_{07} follows in similar fashion. Equation (44) represents the mass-weighted average of resulting stagnation pressure that will be present once the streams are mixed completely. Isolating P_{07} to one side yields equation (45), where $\frac{\dot{m}_6}{\dot{m}_7}$ and $\frac{\dot{m}_8}{\dot{m}_7}$ are defined as follows in equations (46) and (47) respectively.

$$\dot{m}_8 P_{08} + \dot{m}_6 P_{06} = \dot{m}_7 P_{07} \quad (44)$$

$$P_{07} = P_{08}\left(\frac{\dot{m}_8}{\dot{m}_7}\right) + P_{06}\left(\frac{\dot{m}_6}{\dot{m}_7}\right) \quad (45)$$

$$\frac{\dot{m}_6}{\dot{m}_7} = \frac{\dot{m}_{core}+\dot{m}_{f1}}{\dot{m}_{core}+\dot{m}_{aux}+\dot{m}_{ftot}} \quad (46)$$

$$\frac{\dot{m}_8}{\dot{m}_7} = \frac{\dot{m}_{aux}+\dot{m}_{f2}}{\dot{m}_{core}+\dot{m}_{aux}+\dot{m}_{ftot}} \quad (47)$$

The next step is to divide both the numerators and the denominators of equations (47) and (47) by $\dot{m}_{core}$ to yield equations (48) and (49). Then, plug (48) and (49) into (45) to yield (50). Finally, simplify (50) to yield mass-weighted average stagnation pressure of the mixed stream in equation (51).

$$\frac{\dot{m}_6}{\dot{m}_7} = \frac{\dot{m}_{core}/\dot{m}_{core}+\dot{m}_{f1}/\dot{m}_{core}}{\dot{m}_{core}/\dot{m}_{core}+\dot{m}_{aux}/\dot{m}_{core}+\dot{m}_{f1}/\dot{m}_{core}+\dot{m}_{f2}/\dot{m}_{core}} = \frac{(1+f_{actual})}{[1+B+f_{actual}+(B*f_{aux})]} \quad (48)$$

$$\frac{\dot{m}_8}{\dot{m}_7} = \frac{\dot{m}_{aux}/\dot{m}_{core}+\dot{m}_{f2}/\dot{m}_{cor}}{\dot{m}_{core}/\dot{m}_{core}+\dot{m}_{aux}/\dot{m}_{core}+\dot{m}_{f1}/\dot{m}_{core}+\dot{m}_{f2}/\dot{m}_{core}} = \frac{[B+(B*f_{aux})]}{[1+B+f_{actual}+(B*f_{aux})]} \quad (49)$$

$$P_{07} = P_{08}\left(\frac{[B+(B*f_{aux})]}{[1+B+f_{actual}+(B*f_{aux})]}\right) + P_{06}\left(\frac{(1+f_{actual})}{[1+B+f_{actual}+(B*f_{aux})]}\right) \quad (50)$$

$$P_{07} = \frac{B(1+f_{aux})P_{08}+(1+f_{actual})\,P_{06}}{B(1+\,f_{aux})+(1+f_{actual})} \quad (51)$$

Once the two streams have mixed into one, the new stream will exit through a converging nozzle. In equation (52), a ratio is set up to test if the nozzle is choked. If P^*/P_{07} is greater than or equal to P_a/P_{07}, then the nozzle is choked meaning the Mach number at the exit is 1. Subsequently, equations (53) to (56) calculate the exit flow static pressure, static temperature, density, and velocity, respectively.

$$\frac{P^*}{P_{07}} = \left\{1 - \frac{1}{\eta_N}\left[1 - \left(\frac{2}{\gamma_g - 1}\right)\right]\right\}^{\frac{\gamma_g}{\gamma_g - 1}} \quad (52)$$

$$P_e = P_{07}\left(\frac{P^*}{P_{07}}\right) \quad (53)$$

$$T_e = T_{07}\left(\frac{2}{\gamma_g + 1}\right) \quad (54)$$

$$\rho_e = \frac{P_e}{R_g \cdot T_e} \quad (55)$$

$$V_e = M_e\sqrt{\gamma_g \cdot R_g \cdot T_e} \quad (56)$$

Conversely, if P^*/P_{07} is less than or equal to P_a/P_{07}, then the nozzle is not choked. This means that the exit pressure is equal to the ambient pressure. The exit flow conditions for the static temperature, density, Mach number, and velocity are calculated in equations (57) to (60).

$$T_e = T_{07}\left\{1 - \eta_N\left[1 - \left(\frac{P_e}{P_{07}}\right)^{\frac{\gamma_g - 1}{\gamma_g}}\right]\right\} \quad (57)$$

$$\rho_e = \frac{P_e}{R_g \cdot T_e} \tag{58}$$

$$M_e = \sqrt{\left[\left(\frac{T_{07}}{T_e}\right) - 1\right]\left(\frac{2}{\gamma_g + 1}\right)} \tag{59}$$

$$V_e = M_e \sqrt{\gamma_g \cdot R_g \cdot T_e} \tag{60}$$

The last step of this parametric study is to calculate the performance and efficiency of this engine. Equations (61) and (62) calculate Fs and TSFC. In equation (63), the heating value of the fuel is converted from kJ/kmol to J/kg. Lastly, equations (64) to (66) are used to calculate the propulsive, thermal, and overall efficiency, respectively. Conventionally, propulsive efficiency is defined as the ratio of thrust power to the rate of addition of kinetic energy, and thermal efficiency is defined as the ratio of the rate of addition of kinetic energy to the rate of total energy consumption. These are approximations that neglect to account for the rate of addition of pressure energy [13]. Since the TurboAux is utilizing a purely converging nozzle which has choked flow in every case studied, the pressure energy is not negligible. It was necessary to adjust the conventional equations for propulsive and thermal efficiency to account for the increase in pressure energy. This is outlined in equations (64) and (66).

$$F_s = [(1 + f_o)V_e - V_a] + \left[(P_e - P_a)\left(\frac{1 + f_o}{\rho_e \cdot V_e}\right)\right] \tag{61}$$

$$TSFC = \frac{3600 \cdot f_o}{F_s} \tag{62}$$

$$HV = \frac{-Hrp_f \cdot 1000}{M_{fuel}} \tag{63}$$

$$\eta_{prop} = \frac{F_s \cdot V_a}{\left[(1 + f_o)\frac{V_e^2}{2} - \frac{V_a^2}{2}\right] + \left[(P_e - P_a)\left(\frac{1 + f_o}{\rho_e \cdot V_e}\right)\right]^2} \tag{64}$$

$$\eta_{th} = \frac{\left[(1+f_o)\frac{V_e{}^2}{2} - \frac{V_a{}^2}{2}\right] + \left[(P_e - P_a)\left(\frac{1+f_o}{\rho_e \cdot V_e}\right)\right]^2}{f_o \cdot HV} \tag{65}$$

$$\eta_o = \eta_{prop} \cdot \eta_{th} = \frac{F_s \cdot V_a}{f_o \cdot HV} \tag{66}$$

Formulation for the Turbojet Engine with an Afterburner

Every engine in this study shares equations (1) through (6) for the calculations from the inlet up until the LPC. The turbojet however, not having a bypass stream, differs slightly moving forward. Equation (67) calculates the work required to operate the LPC. Equations (10) through (20) and (22) also apply for the turbojet as well as the TurboAux.

$$W_C^{LP} = C_{p0a} \cdot (T_{01} - T_{02}) \tag{67}$$

The equations presented for characterizing the flow through the stages of the turbine, (25) through (28), are also applicable for the turbojet. Where the turbojet diverges is in the calculations modeling the afterburner segment. To compare this afterburner to the auxiliary combustion chamber in the TurboAux, the same combustion temperature of 2516 K has been adopted for the products of the reaction. The combustion process is also modeled the same using the same fuel and equations for calculating the specific enthalpies. Equation (68) is defined as the inverse of equation (18) and represents the number of kilomoles of fuel burned in the main combustion chamber per 1 kilomole of O_2 ingested. Equation (69) represents the number of additional kilomoles of fuel burned per 1 kilomole of O_2 ingested.

$$x = \frac{1}{y} \tag{68}$$

$$z = \frac{[(3.76)\Delta\bar{h}_{N_2} + \Delta\bar{h}_{O_2}] + x[(MC)\Delta\bar{h}_{CO_2} + \left(\frac{MH}{2}\right)\Delta\bar{h}_{H_2O} - (Y_{cc})\Delta\bar{h}_{O_2}]}{-Hrp_f - (MC)\Delta\bar{h}_{CO_2} - \left(\frac{MH}{2}\right)\Delta\bar{h}_{H_2O} + (Y_{cc})\Delta\bar{h}_{O_2}} \quad (69)$$

To calculate any frictional stagnation pressure losses, equation (70) accounts for the efficiency of the burner. Equation (71) is used to calculate the overall fuel to air ratio of the entire engine which will be used in the calculations of Fs and TSFC.

$$P_{07} = P_{06} \cdot (\eta_b) \quad (70)$$

$$f_o = \left(\frac{x}{\eta_b} + \frac{z}{\eta_b}\right)\left(\frac{M_{fuel}}{4.76 \cdot M_{air}}\right) \quad (71)$$

The equations to check the flow at the nozzle and to calculate the flow characteristics at the exit are the same for the turbojet as well as equations (61) through (66) to calculate the performance of the engine.

Formulation for the Turbofan Engine with an Afterburner

Since the TurboAux is modeled as an adaption to the turbofan, it is no surprise that almost all the equations modeling the turbofan are the same aside from a few. Starting at the inlet, equations (1) through (7) are identical. Equation (72) accounts for the 2% loss in stagnation pressure in the fan chute where combustion occurs in the TurboAux. Since no combustion occurs in the fan chute and it is adiabatic, equation (73) shows there is no change in the stagnation temperature from station 2 to 8. The combustion process, the turbine calculations, and the stream mixing calculations remain unchanged. The turbofan then adopts a similar afterburner modeling from the turbojet, but it is imperative to account for the excess oxygen entering the afterburner from the bypass stream. Equation (74) appropriately accounts for this.

$$P_{08} = P_{02} \cdot (\eta_f) \tag{72}$$

$$T_{08} = T_{02} \tag{73}$$

$$x = \left(\frac{1}{y}\right)\left(\frac{1}{B+1}\right) \tag{74}$$

The derivation of T_{07} and P_{07} follow a very similar process as presented for the TurboAux apart from having to account for the auxiliary combustion process. Equation (75) defines k, and equations (75) and (76) are the equations used to calculate those stagnation quantities. Again, equation (77) accounts for the efficiency of the burner and calculates the change in stagnation pressure after the combustion process. Lastly, equation (78) is used to calculate the overall fuel to air ratio to calculate Fs and TSFC as well as the engine efficiencies, and the equations to check the flow at the nozzle and to calculate the flow characteristics at the exit are again the same for the turbofan as well.

$$k = \frac{C_{poa}}{C_{pog}} \tag{75}$$

$$T_{07} = \frac{T_{08}(B \cdot \mathrm{k}) + T_{06}(1+f_{actual})}{(B \cdot k)+(1+f_{actual})} \tag{76}$$

$$P_{07} = \frac{P_{08} \cdot B + P_{06}(1+f_{actual})}{(\mathrm{B}+1+f_{actual})} \tag{77}$$

$$P_{09} = P_{07} \cdot (\eta_b) \tag{78}$$

$$f_o = \left(\frac{x}{\eta_b} + \frac{z}{\eta_b}\right)\left(\frac{M_{fuel}}{4.76 \cdot M_{air}}\right) \tag{79}$$

In the following chapter, the results and performance of these engines will be presented and discussed in comparison with one another.

CHAPTER IV

RESULTS AND DISCUSSION

In this chapter, the comparative results and performances of the engines studied are presented and compared. Tables 6-8 summarize the analysis and performance the various engine configurations. The full results tables can be found in the Appendix G.

Table 6. Performance Results at BPR of 0.1

Engine	Turbojet with Afterburning	Turbofan with Afterburning	TurboAux
FPR	7	7	7
Bypass Ratio	N/A	0.1	0.1
Fs	1319.787153	1309.831555	868.3308192
TSFC	0.1923519	0.194079469	0.12999793
Propulsive Efficiency	45.23%	45.60%	59.48%
Thermal Efficiency	25.72%	25.29%	28.94%
Overall Efficiency	11.64%	11.53%	17.22%

Table 7. Performance Results at BPR of 0.8

Engine	Turbojet with Afterburning	Turbofan with Afterburning	TurboAux
FPR	7	7	7
Bypass Ratio	N/A	0.8	0.8
Fs	1319.787153	1261.226815	983.7361302
TSFC	0.1923519	0.204136861	0.163484892
Propulsive Efficiency	45.23%	47.41%	55.62%
Thermal Efficiency	25.72%	23.12%	24.61%
Overall Efficiency	11.64%	10.96%	13.69%

Table 8. Performance Results at BPR of 1.5

Engine	Turbojet with Afterburning	Turbofan with Afterburning	TurboAux
FPR	5.3	5.3	5.3
Bypass Ratio	N/A	1.5	1.5
Fs	1319.826856	1214.235908	1014.266203
TSFC	0.192402496	0.213796329	0.18240472
Propulsive Efficiency	45.23%	49.11%	55.04%
Thermal Efficiency	25.72%	21.32%	22.29%
Overall Efficiency	11.63%	10.47%	12.27%

Figures 23 to 27 below are each of the individual performance parameters and how they varied across each BPR-FPR configuration. It is important to note that these parameters are not only affected by BPR, but rather the optimal BPR-FPR configuration combination that was obtained from the optimization analysis.

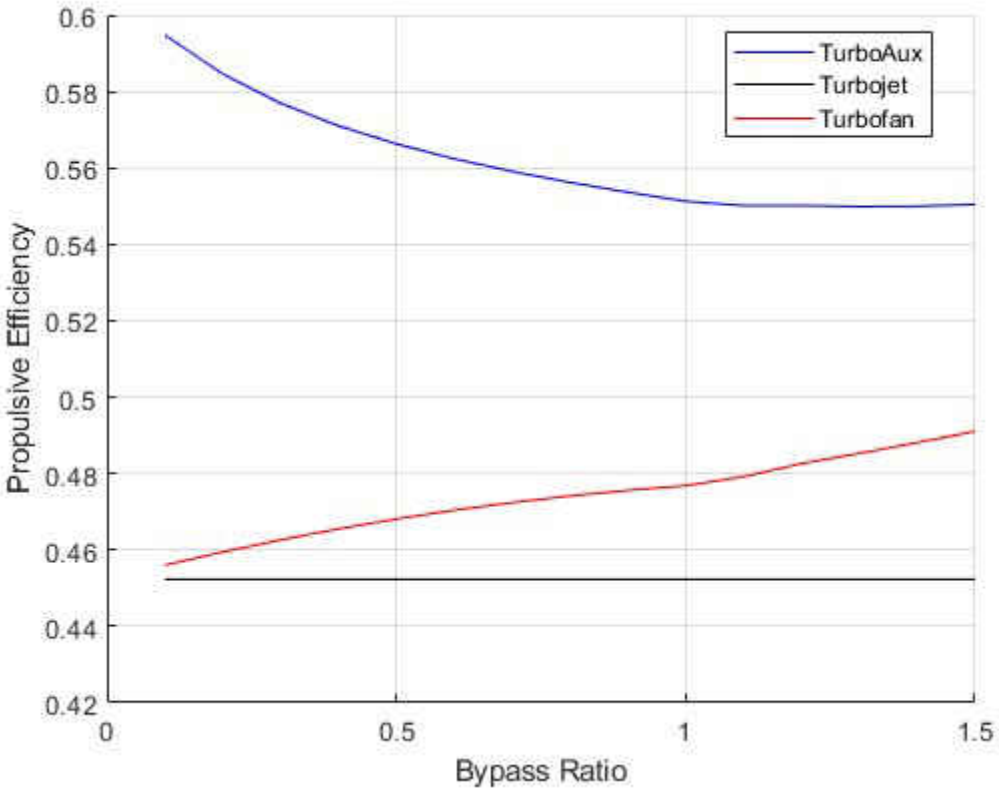

Figure 23. Propulsive Efficiency vs. Bypass Ratio

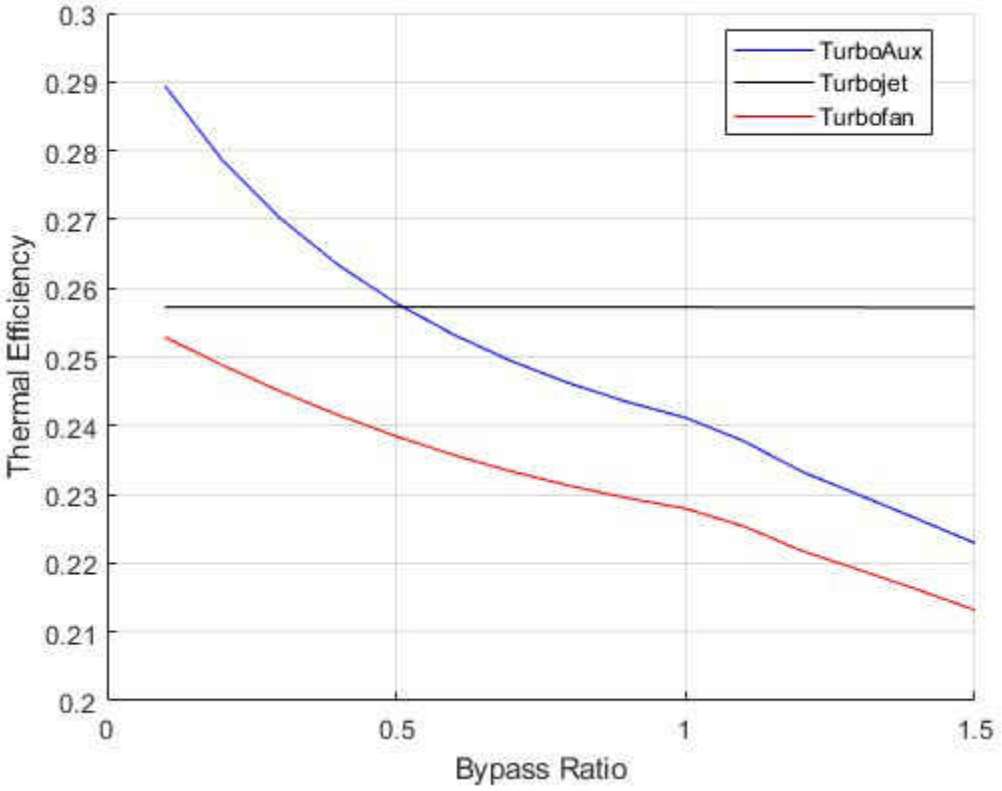

Figure 24. Thermal Efficiency vs. Bypass Ratio

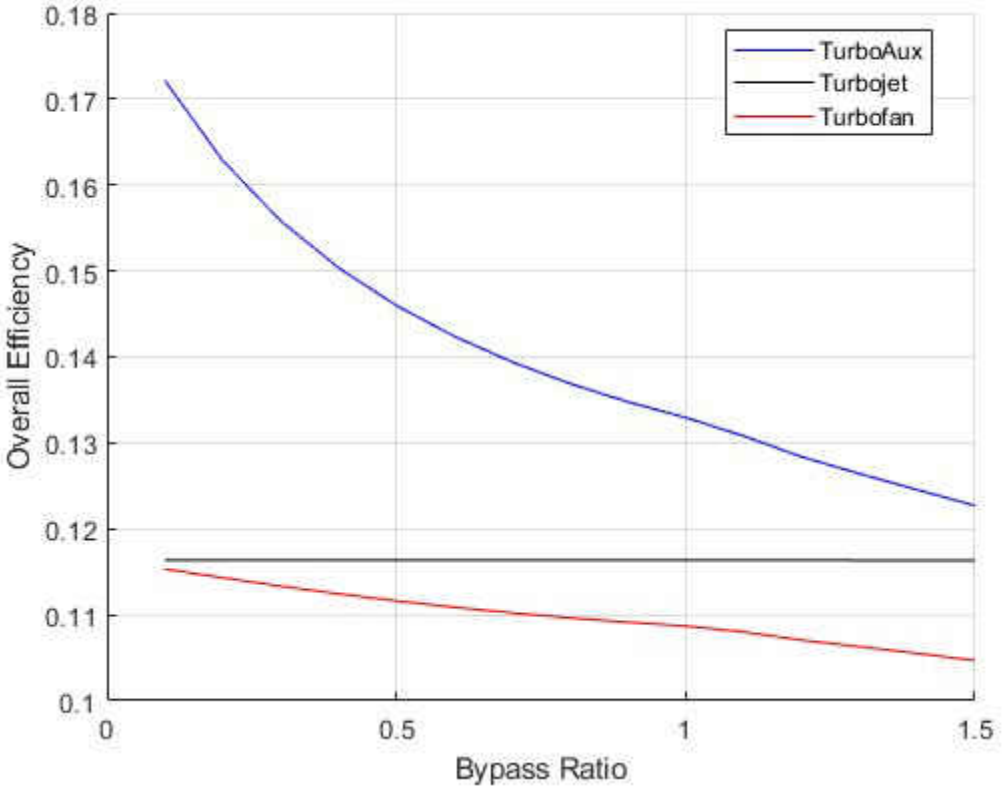

Figure 25. Overall Efficiency vs. Bypass Ratio

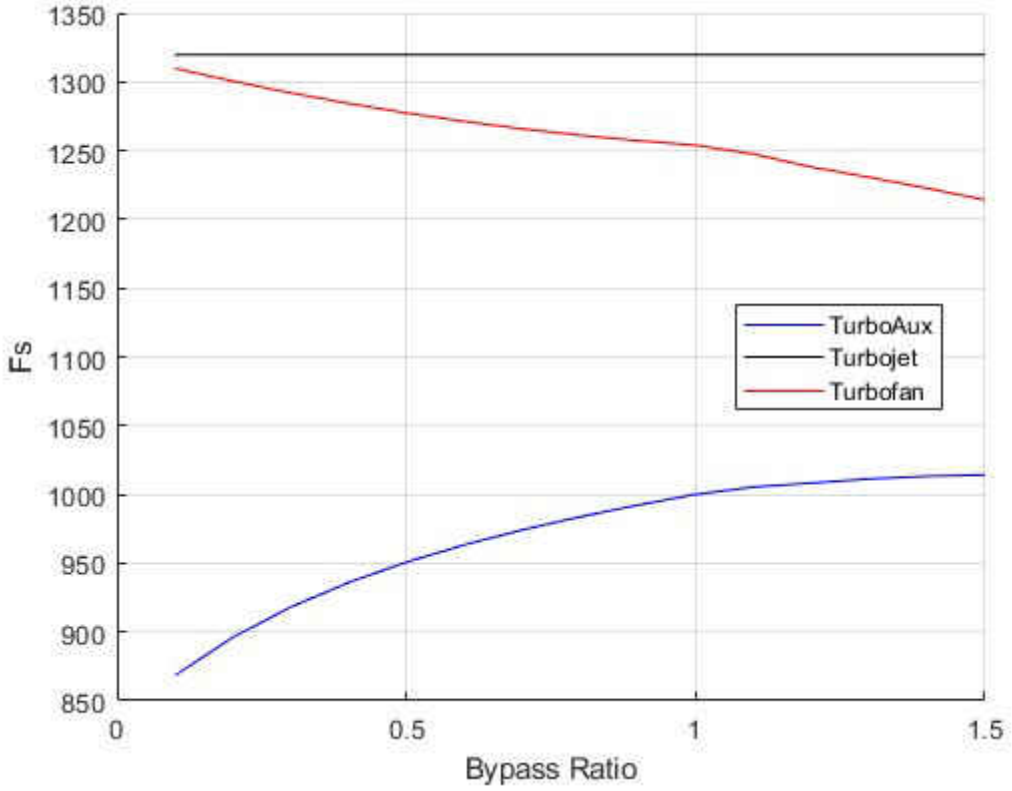

Figure 26. Fs vs. Bypass Ratio

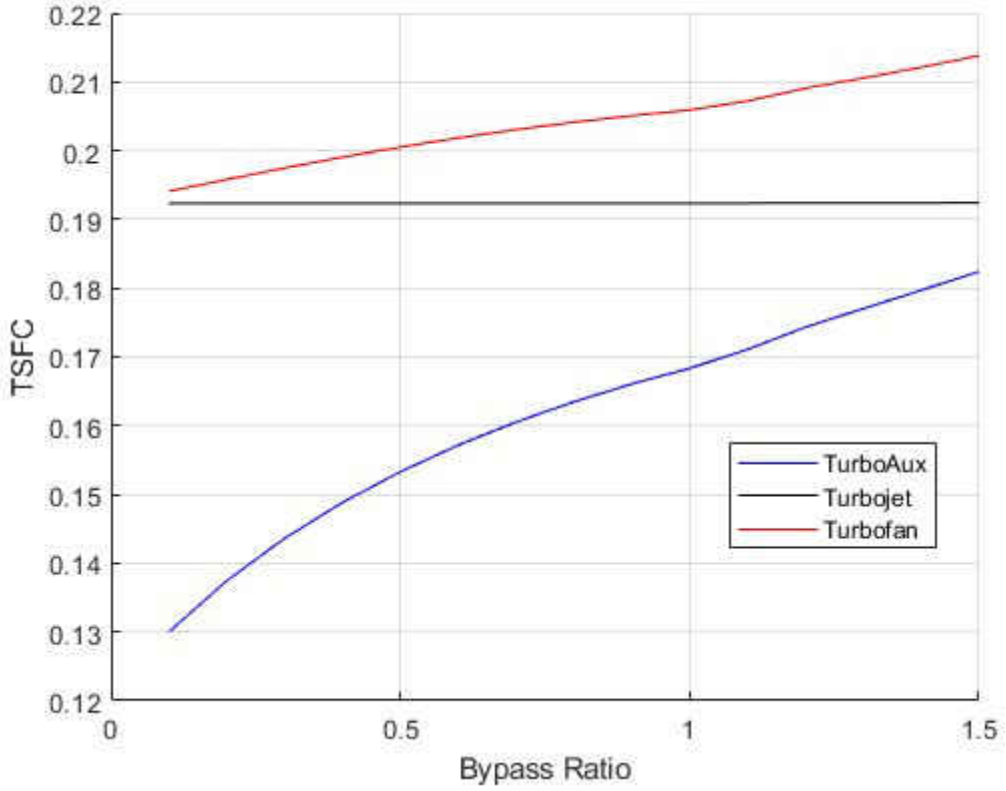

Figure 27. TSFC vs. Bypass Ratio

These results illustrate many notable trends. Firstly, the plots of the performance parameters for the turbojet show very little to no variation across the optimal designs. This can be attributed to FPR being the only variable in the turbojet analysis. As aforementioned, with OPR and TINT fixed, the energy input of the engine is fixed, and since a turbojet engine does not have a bypass stream, the slight variation in the FPR values proved inconsequential to the performance of the engine. Secondly, the turbojet also produced the most specific thrust of the three engines, and while the turbofan outperformed the turbojet with respect to TSFC when compared without afterburner segments in either engine, when an afterburner was augmented, the turbofan produced less Fs and exhibited an increase in TSFC. While this may be an unfavorable trend at first glance, after closer investigation, it is apparent that the increase in

TSFC is attributed to the increase in BPR. As BPR increases, the ratio of fresh air from the fan chute to oxygen-depleted air from the combustion chamber increases, thus lowering the stagnation temperature of the mixed stream. This means more fuel must be burned to reach a combustion temperature of 2516 K. For example, at a BPR of 0.1, T_{07}, the stagnation temperature of the mixed stream is 1224.8 K, conversely at a BPR of 1.5, T_{07} is 735.7 K.

Another trend observed of the turbofan was an increase in propulsive efficiency and a decrease in thermal efficiency. The overall efficiency, which is a product of the propulsive and thermal efficiencies showed a decrease as well. These trends were expected. Propulsive efficiency is defined as the ratio of thrust power to the rate of addition of energy to the propellant, and the rate at which thrust power decreased was less than the rate at which energy was added to the propellant with the addition of the afterburner segment. As mentioned in previous chapters, the reheat cycle proves detrimental to the thermal efficiency, due to its high fuel consumption, despite augmenting a significant amount of thrust.

The TurboAux exhibited interesting trends as well. The TurboAux delivered much higher propulsive efficiency in comparison to the other engines. This can be attributed to the increase in BPR which also allows more mass to flow into the auxiliary combustion chamber. However, although producing a higher thermal efficiency than the turbofan, the TurboAux exhibited a similar declining trend across the optimal configurations. This too can be attributed to the increase in fuel consumption. In terms of Fs, the TurboAux greatly underperformed the other two engines, but drastically outperformed the other two engines with respect to TSFC. This was especially evident at lower BPRs where the fraction of the mass flow entering the auxiliary combustion chamber is much smaller than that of the core stream.

Although these trends of the TurboAux show a promising future, it is important to compare the performance of this engine with current operational engines. The next chapter will compare the TurboAux and its performance not on specific quantities, such as Fs, but total quantities such as actual thrust. This will be useful in understanding the application range of this engine and make a case for its use in specific industries. To gather a full understanding, the TurboAux should be analyzed with computational fluid dynamics in future study.

CHAPTER V

APPLICATIONS AND EXAMPLES- UTILITY AND TRADE STUDY

In this chapter, the TurboAux is compared to other engines from industry. The engines that were selected as comparison, were selected to make a case for the TurboAux to possibly be used in their place. The engines selected are mainly low-bypass turbofan engines, with a few high-bypass turbofan engines, that have BPRs between 0.1 and 1.9 aside from the two exceptions, and have applications ranging from military aircraft to business jets for private flights. For some of the military aircraft, it was exceedingly difficult to find certain operating parameters due to the classified nature of their design and operation, but the information presented comes from literature [14,15]. All other sources of data will be cited in the References chapter of this paper [16-24]. The engine selected are:

- Pratt & Whitney F100 (afterburning military engine used in F-16)
- Pratt & Whitney JT8D-1 (commercial engine used in B727)
- General Electric F404 (afterburning military engine used in F-117 Nighthawk)
- General Electric F110 (afterburning military engine used in F-16 Fighting Falcon)
- General Electric TF34 (military engine used in A-10 Thunderbolt II)
- General Electric CF34 (civilian variant of TF34 used in business jets)
- Rolls Royce SPEY512 (afterburning military engine used in F-4 Phantom II)

TurboAux Utility Study

Table 9 is a representation of the design points and performances of these engines. After finding and tabulating the design and performance parameters, these engines were separately compared to the turbofan for the “dry” cases and the TurboAux for the “wet” cases. It is

important to remember that the TurboAux is simply an extension of the turbofan. What that means is that the TurboAux can be operated as a pure turbofan when the auxiliary combustion chamber is not switched on, but can also be operated as the TurboAux when the auxiliary combustion chamber is switched on; much like a military turbofan being able to turn on and turn off the afterburner.

The actual thrust of the turbofan and TurboAux was calculated by multiplying the Fs by the specific engine's mass flow rate. From there, the fuel mass flow rate was calculated by multiplying the thrust by the TSFC. The "wet" and "dry" subscripts are used to denote when the afterburner and auxiliary combustion chamber are in use and when they are not, respectively. These calculations indicate how much thrust and how much fuel the TurboAux would produce and consume if it were to operate at the same mass flow rate. Tables 10 through 16 show the results of this comparison.

Table 9. Specific Engine Operation and Performance Data

Engine	**BPR**	**$\dot{m}$ (kg/s)**	**T_{dry} (kN)**	**T_{wet} (kN)**	**$TSFC_{dry}$ (kg/N*hr)**	**$TSFC_{wet}$ (kg/N*hr)**
P&W F100	0.63	102	64.9	105.7	0.074	0.19750
P&W JT8D-1	1.1	143	62.3	N/A	0.059652	N/A
GE F404	0.3	63.5	48.9	78.7	0.082603	0.177442
GE F110	0.8	123	81.5	129	0.069345	0.193759
GE TF34	6.2	153	40	N/A	0.037834	N/A
GE CF34	6.3	139	35.5	N/A	0.036648	N/A
RR SPEY	0.7	93	55.6	91.2	0.061236	0.198858

Table 10. Thrust Performance Specifications of P&W F100 and a TurboAux Equivalent

Engine	**BPR**	**$\dot{m}_{air}$ (kg/s)**	**$\dot{m}_{fdry}$ (kg/s)**	**$\dot{m}_{fwet}$ (kg/s)**	**T_{dry} (kN)**	**T_{wet} (kN)**	**$TSFC_{dry}$ (kg/N*hr)**	**$TSFC_{wet}$ (kg/N*hr)**
TurboAux	0.6	102	1.78	4.29	65.2	98.3	0.098	0.157
P&W F100	0.63	102	1.33	5.80	64.9	105.7	0.074	0.198

Table 11. Thrust Performance Specifications of P&W JT8D-1 and a TurboAux Equivalent

Engine	**BPR**	**$\dot{m}_{air}$ (kg/s)**	**$\dot{m}_{fdry}$ (kg/s)**	**$\dot{m}_{fwet}$ (kg/s)**	**T_{dry} (kN)**	**T_{wet} (kN)**	**$TSFC_{dry}$ (kg/N*hr)**	**$TSFC_{wet}$ (kg/N*hr)**
TurboAux	1.1	143	1.90	6.83	78.7	143.8	0.087024	0.171098
P&W JT8D-1	1.1	143	1.03	N/A	62.3	N/A	0.059652	N/A

Table 12. Thrust Performance Specifications of GE F404 and a TurboAux Equivalent

Engine	**BPR**	**$\dot{m}_{air}$ (kg/s)**	**$\dot{m}_{fdry}$ (kg/s)**	**$\dot{m}_{fwet}$ (kg/s)**	**T_{dry} (kN)**	**T_{wet} (kN)**	**$TSFC_{dry}$ (kg/N*hr)**	**$TSFC_{wet}$ (kg/N*hr)**
TurboAux	0.3	63.5	1.36	2.33	45.6	58.3	0.107705	0.143615
GE F404	0.3	63.5	1.12	3.88	48.9	78.7	0.082603	0.177442

Table 13. Thrust Performance Specifications of GE F110 and a TurboAux Equivalent

Engine	BPR	$\dot{m}_{air}$ (kg/s)	$\dot{m}_{fdry}$ (kg/s)	$\dot{m}_{fwet}$ (kg/s)	T_{dry} (kN)	T_{wet} (kN)	$TSFC_{dry}$ (kg/N*hr)	$TSFC_{wet}$ (kg/N*hr)
TurboAux	0.8	123	1.91	5.49	73.7	121	0.093274	0.163485
GE F110	0.8	123	1.57	6.94	81.5	129	0.069345	0.193759

Table 14. Thrust Performance Specifications of GE TF34 and a TurboAux Equivalent

Engine	BPR	$\dot{m}_{air}$ (kg/s)	$\dot{m}_{fdry}$ (kg/s)	$\dot{m}_{fwet}$ (kg/s)	T_{dry} (kN)	T_{wet} (kN)	$TSFC_{dry}$ (kg/N*hr)	$TSFC_{wet}$ (kg/N*hr)
TurboAux	1.5	153	1.71	7.86	75.3	155.2	0.081832	0.182405
GE TF34	6.2	153	0.42	N/A	40	N/A	0.037834	N/A

Table 15. Thrust Performance Specifications of GE CF34 and a TurboAux Equivalent

Engine	BPR	$\dot{m}_{air}$ (kg/s)	$\dot{m}_{fdry}$ (kg/s)	$\dot{m}_{fwet}$ (kg/s)	T_{dry} (kN)	T_{wet} (kN)	$TSFC_{dry}$ (kg/N*hr)	$TSFC_{wet}$ (kg/N*hr)
TurboAux	1.5	139	1.55	7.14	68.4	141	0.081832	0.182405
GE CF34	6.3	139	0.42	N/A	35.5	N/A	0.036648	N/A

Table 16. Thrust Performance Specifications of RR SPEY and a TurboAux Equivalent

Engine	BPR	$\dot{m}_{air}$ (kg/s)	$\dot{m}_{fdry}$ (kg/s)	$\dot{m}_{fwet}$ (kg/s)	T_{dry} (kN)	T_{wet} (kN)	$TSFC_{dry}$ (kg/N*hr)	$TSFC_{wet}$ (kg/N*hr)
TurboAux	0.7	93	1.53	4.04	57.5	90.6	0.095729	0.160539
RR SPEY	0.7	93	0.95	5.04	55.6	91.2	0.061236	0.198858

In Tables 11, 14, and 15, the TurboAux is compared to engines without afterburners, but the results of the TurboAux while the auxiliary combustion chamber is activated are included to make a case for its use as a turbofan engine but if more thrust production is required, the auxiliary combustion process can be turned on. In the comparison of the TurboAux to the GE TF34 and the civilian variant GE CF34 specifically, the GE engines both have BPRs much higher than the TurboAux so the highest BPR configuration of 1.5 was selected to compare against those engines.

In contrast, another comparison studied is one where the TurboAux net thrust is set equal to the net thrust of the engines it is being compared to. From this, the inlet mass flow rate required to achieve that net thrust quantity, for both dry and wet operation, is calculated. Using those mass flow rates, and since the ambient conditions are already specified, the required engine diameters are calculated for both instances. This calculation indicates how large the TurboAux engine inlet must be and how much mass flow it must consume to produce the same net thrust as the engines it is being compared to. Tables 17 through 23 present the results of this comparison.

Table 17. Size Specifications of P&W F100 and a TurboAux Equivalent

Engine	**BPR**	**T_{dry} (kN)**	**T_{wet} (kN)**	**$\dot{m}_{air}$ (kg/s)**	**$\dot{m}_{air}$ (dry) (kg/s)**	**$\dot{m}_{air}$ (wet) (kg/s)**	**D_{actual} (m)**	**D_{dry} (m)**	**D_{wet} (m)**
TurboAux	0.6	64.9	105.7	N/A	101.6	109.7	N/A	0.808	0.839
P&W F100	0.63	64.9	105.7	102	102	102	0.884	0.884	0.884

Table 18. Size Specifications of P&W JT8D-1 and a TurboAux Equivalent

Engine	**BPR**	**T_{dry} (kN)**	**T_{wet} (kN)**	**$\dot{m}_{air}$ (kg/s)**	**$\dot{m}_{air}$ (dry) (kg/s)**	**$\dot{m}_{air}$ (wet) (kg/s)**	**D_{actual} (m)**	**D_{dry} (m)**	**D_{wet} (m)**
TurboAux	1.1	62.3	N/A	N/A	113.2	N/A	N/A	0.853	N/A
P&W JT8D-1	1.1	62.3	N/A	143	143	143	1.143	1.143	N/A

Table 19. Size Specifications of GE F404 and a TurboAux Equivalent

Engine	**BPR**	**T_{dry} (kN)**	**T_{wet} (kN)**	**$\dot{m}_{air}$ (kg/s)**	**$\dot{m}_{air}$ (dry) (kg/s)**	**$\dot{m}_{air}$ (wet) (kg/s)**	**D_{actual} (m)**	**D_{dry} (m)**	**D_{wet} (m)**
TurboAux	0.3	48.9	78.7	N/A	68.1	85.7	N/A	0.661	0.742
GE F404	0.3	48.9	78.7	63.5	63.5	63.5	0.889	0.889	0.889

Table 20. Size Specifications of GE F110 and a TurboAux Equivalent

Engine	BPR	T_{dry} (kN)	T_{wet} (kN)	$\dot{m}_{air}$ (kg/s)	$\dot{m}_{air}$ (dry) (kg/s)	$\dot{m}_{air}$ (wet) (kg/s)	D_{actual} (m)	D_{dry} (m)	D_{wet} (m)
TurboAux	0.8	81.5	129	N/A	136.1	131.1	N/A	0.935	0.918
GE F110	0.8	81.5	129	123	123	123	1.181	1.181	1.181

Table 21. Size Specifications of GE TF34 and a TurboAux Equivalent

Engine	BPR	T_{dry} (kN)	T_{wet} (kN)	$\dot{m}_{air}$ (kg/s)	$\dot{m}_{air}$ (dry) (kg/s)	$\dot{m}_{air}$ (wet) (kg/s)	D_{actual} (m)	D_{dry} (m)	D_{wet} (m)
TurboAux	1.5	40	N/A	N/A	81.3	N/A	N/A	0.723	N/A
GE TF34	6.2	40	N/A	153	153	153	1.27	1.27	N/A

Table 22. Size Specifications of GE CF34 and a TurboAux Equivalent

Engine	BPR	T_{dry} (kN)	T_{wet} (kN)	$\dot{m}_{air}$ (kg/s)	$\dot{m}_{air}$ (dry) (kg/s)	$\dot{m}_{air}$ (wet) (kg/s)	D_{actual} (m)	D_{dry} (m)	D_{wet} (m)
TurboAux	1.5	35.5	N/A	N/A	72.2	N/A	N/A	0.681	N/A
GE CF34	6.3	35.5	N/A	139	139	139	1.24	1.24	N/A

Table 23. Size Specifications of RR SPEY and a TurboAux Equivalent

Engine	BPR	T_{dry} (kN)	T_{wet} (kN)	$\dot{m}_{air}$ (kg/s)	$\dot{m}_{air}$ (dry) (kg/s)	$\dot{m}_{air}$ (wet) (kg/s)	D_{actual} (m)	D_{dry} (m)	D_{wet} (m)
TurboAux	0.7	55.6	91.2	N/A	90	93.6	N/A	0.760	0.775
RR SPEY	0.7	55.6	91.2	93	93	93	0.99	0.99	0.99

After conducting this comparison analysis on the assumption of equal inlet mass flow rates, a few trends became apparent. When operated in "dry" conditions (when the auxiliary combustion process is inactive), the TurboAux exhibited higher fuel consumption rates. This was evident in every case the TurboAux was compared on an equal inlet mass flow rate basis. When compared with the P&W F100 engine, the TurboAux configuration chosen as comparison was at a BPR of 0.6 versus the F100 operating at 0.63, but this small difference in BPR did not seem to cause much of an effect as the TurboAux produced roughly the same amount of dry thrust as the F100. When compared to the commercial P&W JT8D-1 engine, the TurboAux produced greater dry net thrust, but at the cost of higher fuel consumption. The comparison of the TurboAux to the GE TF34 and CF34 however do not provide much insight as to how the TurboAux matches up since their operating BPRs are much different. The comparison between the TurboAux and the RR SPEY showed almost identical net thrust production under both dry and wet operation. The fuel mass flow rates were comparable as well.

On the assumption of equal net thrust production, the comparison of the TurboAux to these engines would indicate how much mass flow is required, thus indicating how large the inlet would have to be. When compared to the P&W F100, the TurboAux requires about the same

inlet mass flow rate around 102 kg/s, but this number slightly rose when the auxiliary combustion chamber was activated. The inlet size required however was still smaller than that of the F100. Compared to the JT8D-1, both the mass flow rate required, and the minimum size requirement were much smaller than that of the JT8D-1. When compared to both the GE F404 and F110, the TurboAux required greater inlet mass flow and smaller inlet diameter. These contrasting trends could be attributed to differences in ambient conditions as most of these parameters taken from literature do not specify the conditions at which the net thrust, and the inlet mass flow rate are recorded at. Again, comparison of the TurboAux to the TF34 and the CF34 are not quite indicative of much, and further evaluation of the TurboAux at higher BPRs is required. Lastly, the RR SPEY again served as a good comparison to the TurboAux. The RR SPEY operates with an inlet mass flow of 93 kg/s, while the TurboAux running dry requires 90 kg/s. Operating wet, the TurboAux requires 93.6 kg/s compared to the SPEY's 93 kg/s. The required inlet diameter for the dry and wet operation of the TurboAux are 0.76 m and 0.775 m, respectively, compared to the RR SPEY inlet diameter of 0.99 m. A trade study graph based on these operating conditions and results is presented to better understand the TurboAux's use.

Trade Study

The trade study conducted is illustrated in Figures 28 and 29 as a graph of the tradeoff between net thrust and TSFC versus mass flow and bypass ratio. The vertical lines indicate constant BPR whereas the horizontal dotted lines indicate the constant mass flow rates of the engines in the prior comparison. When following the color-coded horizontal line to where it intersects with its color-coded vertical line, it indicates the configuration of a specific engine. Following that same vertical line, the performance of that engine in comparison to the TurboAux is shown. For example, when following the purple horizontal line of a constant mass flow rate of

63.5 kg/s, it intersects with the purple vertical line at a BPR of 0.3. This is the engine configuration of the GE F404. Following that constant BPR line, it shows that the TurboAux produced a little less dry net thrust than the F404 but produced even less wet net thrust in comparison. With respect to TSFC however, it is evident that when operating wet, the TurboAux outperformed the F404. These figures illustrate the tradeoff between net thrust and fuel consumption at specific engine configurations. As aforementioned, when compared to the P&W F100, the TurboAux simulations at a BPR of 0.6 were selected as comparison being that it was the closest configuration to that of the F100. This is evident in the figures as the red squares are not shown exactly on the constant BPR line of 0.63. In the final chapter, the findings and conclusions drawn will be presented along with plans for future work.

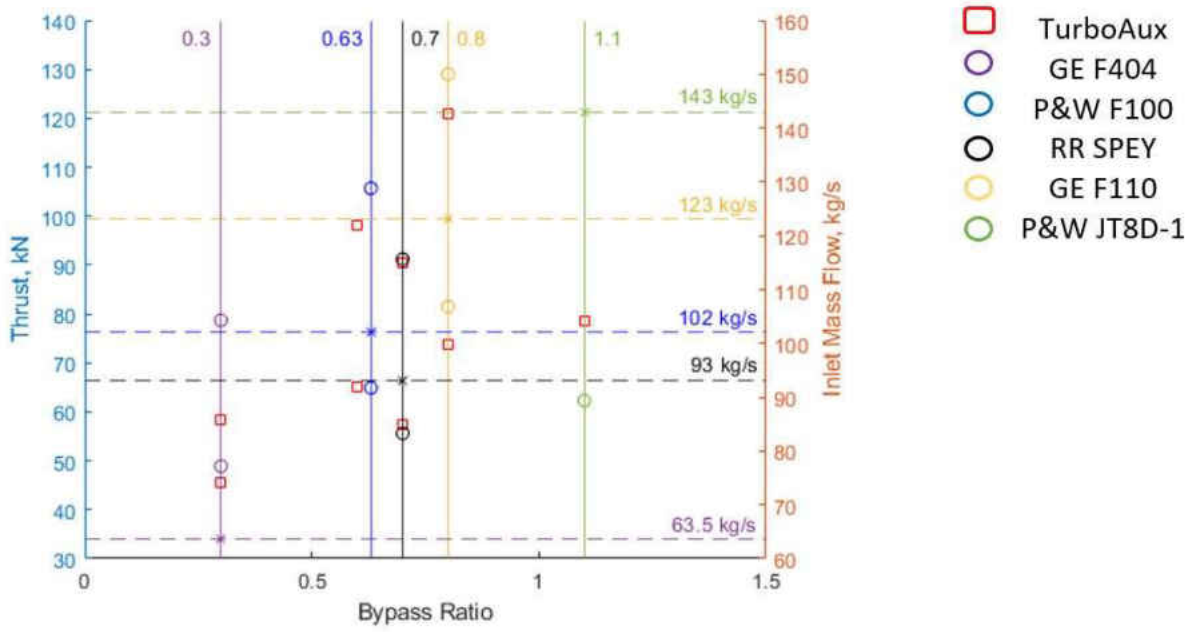

Figure 28. Thrust Trade Study

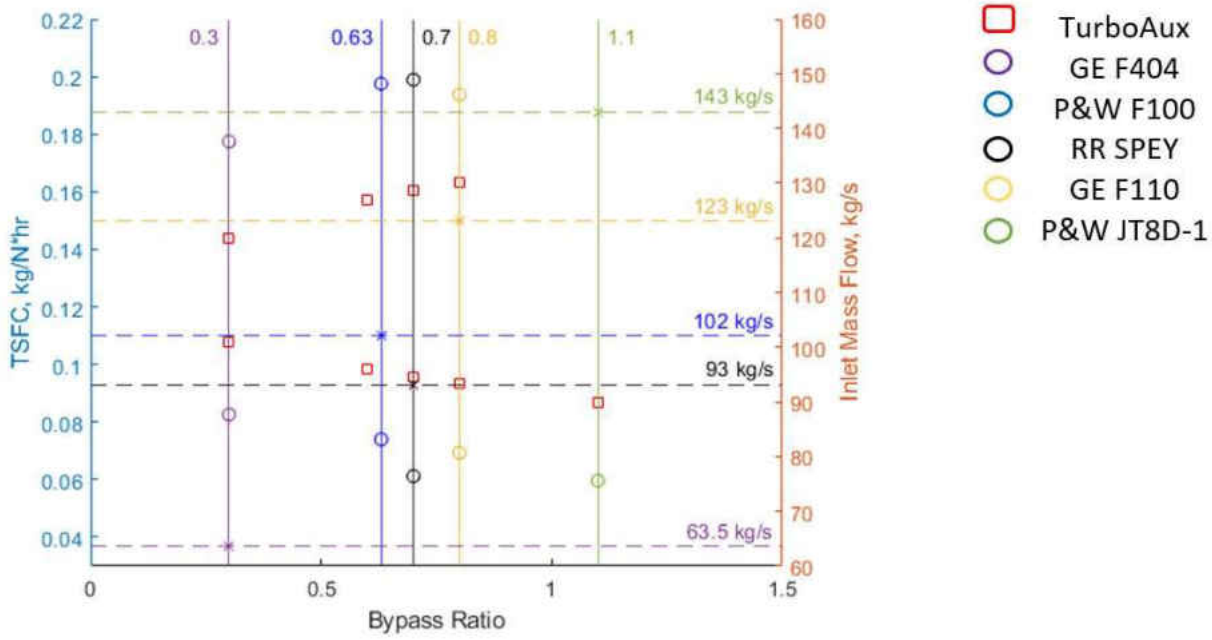

Figure 29. TSFC Trade Study

CHAPTER VI

CONCLUSION AND FUTURE WORK

This research conducted and presented in this paper is an extension of the work done by Asundi and Ali [5]. The novel engine was modeled in MATLAB and was compared to afterburning counterparts of identical design. The TurboAux's design was an effort to optimize the concept of Asundi and Ali's auxiliary high-pressure bypass engine [5]. Upon the analysis to arrive at an optimized design for a range of bypass ratios from 0.1 to 1.5, the TurboAux was compared to turbojet and turbofan engines with afterburning. Across that range of bypass ratios, the TurboAux showed a significant increase in Fs while the turbofan exhibited a sharp decline in Fs. Since it does not have a bypass ratio, the turbojet produced nearly constant numbers for Fs, TSFC, and efficiency across the optimal FPRs. The TurboAux showed to consume less fuel across that same range as well. To further understand how the TurboAux would compare to real engines, it was compared with a variety of engines ranging in uses. In BPRs ranging from 0.1 to 1.5, during wet operation, the TurboAux exhibited net thrust of similar magnitude in comparison to the real engines while requiring less fuel. During dry operation, the TurboAux exhibited net thrust output of similar magnitude but typically at a higher cost in fuel consumption. This puts the TurboAux's niche as a possible replacement for military engines and perhaps a few low-bypass business jet engines.

To better understand the usefulness of the TurboAux, further analysis is required. This further analysis could be investigating whether the TurboAux could serve as a replacement to higher bypass ratio engines with the augmentation of a tertiary compressor or fan accompanied with an additional bypass stream and fan chute around the entire TurboAux, similar to the research conducted by Asundi and Ali. As a future study, the TurboAux configuration could be

further analyzed with computational fluid dynamics to get a deeper understanding of the inner workings of this novel engine.

REFERENCES

[1] Augustyn, A., Shukla, G., and Dixon, L., "Steam engine," Encyclopædia Britannica, UK, 2020. Available: https://www.britannica.com/technology/steam-engine.

[2] Bilstein, R. E., Crouch, T. D., and Boyne, W. J., "History of flight," Encyclopædia Britannica, UK, 2018. Available: https://www.britannica.com/technology/history-of-flight.

[3] Bellis, M., "Who Invented the Jet Engine?," ThoughtCo, USA, 2019. Available: https://www.thoughtco.com/history-of-the-jet-engine-4067905.

[4] Saravanamuttoo, H. I. H., Rogers, G. F. C., and Cohen, H. *Gas Turbine Theory*. Pearson Education, 2001.

[5] Asundi, S. A., and Ali, S. F. Parametric Study of a Turbofan Engine with an Auxiliary High-Pressure Bypass. International Journal of Turbomachinery, Propulsion and Power. 1. Volume 4, 2. http://dx.doi.org/10.3390/ijtpp4010002.

[6] Raymer, D.P., *Aircraft Design: A Conceptual Approach*, 5th ed., AIAA Education Series; American Institute of Aeronautics & Astronautics: Reston, VA, USA, 2012.

[7] MacIsaac, B., and Langston, R., *Gas Turbine Propulsion Systems*, 1st ed., Wiley: Hoboken, NJ, USA, 2011.

[8] Vaferi, K., Vajdi, M., Nekahi, S., Nekahi, S., Moghanlou, F. S., Asl, M. S., and Mohammadi, M. Thermo-Mechanical Simulation of Ultrahigh Temperature Ceramic Composites as Alternative Materials for Gas Turbine Stator Blades. Ceramics International. http://dx.doi.org/10.1016/j.ceramint.2020.08.164.

[9] Jakubowski, R. Evaluation of Performance Properties of Two Combustor Turbofan Engine. Ekspolatacja i Niezawodnosc - Maintenance and Reliability. 4. Volume 17, 575–581. http://dx.doi.org/10.17531/ein.2015.4.13.

[10] Liew, K. H., Urip, E., and Yang, S. L. Parametric Cycle Analysis of a Turbofan Engine with an Interstage Turbine Burner. Journal of Propulsion and Power. 3. Volume 21, 546–551. http://dx.doi.org/10.2514/1.2546.

[11] Lee, A. S., Singh, R., and Probert, S. D. Two-Combustor Engines' Performances Under Design and Off-Design Conditions. 45th AIAA/ASME/SAE/ASEE Joint Propulsion Conference & Exhibit. http://dx.doi.org/10.2514/6.2009-4838.

[12] Campbell, A.S., Thermodynamic Analysis of Combustion Engines, 1st ed., Wiley: Hoboken, NJ, USA, 1979.

[13] Hill, P., and Peterson, C., Mechanics and Thermodynamics of Propulsion, 2nd ed., Prentice Hall, USA, 1992.

[14] Jagtenberg, M. H., "Development of A Preliminary Lifting Analysis Tool for The F135-PW-100 Engine," thesis, Delft University of Technology, 2018.

[15] Bose, T. K., "Appendix: Engine Data Tables," Airbreathing propulsion: An Introduction, New York, NY: Springer, 2012, pp. 267–309.

[16] Camm, F., Santa Monica, "The Development of the FIO00-P W-220 and FII-GE-100 Engines: A Case Study of Risk Assessment and Risk Management," Directorate of Plans, Hq USAF, CA: RAND, 1994.

[17] "Pratt & Whitney F100-PW-220," National Museum of the United States Air Force™ Available: https://www.nationalmuseum.af.mil/Visit/Museum-Exhibits/Fact-Sheets/Display/Article/196437/pratt-whitney-f100-pw-220/.

[18] "JT8D-219 Turbofan Engine," Pratt & Whitney Available: https://web.archive.org/web/20170510125602/http://pw.utc.com/Content/Press_Kits/pdf/me_jt8d-219_pCard.pdf.

[19] "Proven Experience, Program Upgrades Spark GE F110 and F404/414 Popularity," GE Aviation Available: https://web.archive.org/web/20100929062201/http://geae.com/aboutgeae/presscenter/military/military_20100719.html.

[20] "The F110 Engine," The F110 Engine | GE Aviation Available: https://www.geaviation.com/military/engines/f110-engine.

[21] "TF34 Turbofan Engines," GE Aviation Available: https://www.geaviation.com/sites/default/files/datasheet-TF34_1.pdf.

[22] "The CF34 Engine," GE Aviation Available: https://www.geaviation.com/commercial/engines/cf34-engine.

[24] "The Engine Handbook," Military Turbofan Engine Data Available: https://web.archive.org/web/20180221164359/http://www.aircraftenginedesign.com/TableB2.html.

APPENDICES

Appendix A: MATLAB Code for Turbojet

```
% Pure Turbojet
clc, clear, close all
format longG

%Flight Conditons
Ma = 0.84;
Pa = 54.05;
Ta = 255.7;
OPR = 50;
compLow = [7,7,7,7,7,7,7,7,7,7,6.7,6.2,5.9,5.6,5.3];
compHigh = OPR./compLow;
Rair = 287;
Rgas = Rair;
gamair = 1.4;
gamgas = 1.3333;
Va = Ma*sqrt(gamair*Rair*Ta);
Cpoa = (gamair*Rair)/(gamair-1);
Cpog = (gamgas*Rgas)/(gamgas-1);

%Efficiencies
eta_diff = 0.93;
eta_comp = 0.87;
eta_burn = 0.98;
delta_burn = 0.04;
eta_mech = 0.99;
eta_turb = 0.9;
eta_nozz = 0.95;

%Molecular Weights
Mfuel = 197.7;
Mair = 28.97;
MC = 14.4;
MH = 24.9;
MO = 0;
ycc = MC + (MH/4) - (MO/2);

%Delta h Constants
A = [299180, 309070;
   56835, 93048;
   88923, 154670;
   43388, 127010;
```

```
    31317, 44639];

B = [37.85, 39.29;
    66.27, 68.58;
    49.36, 60.43;
    42.27, 46.25;
    37.46, 39.32];

C = [-4571.9, -6201.9;
    -11634, -16979;
    -7940.8, -19212;
    -6635.4, -18798;
    -4559.3, -6753.4];


%Other Constants
Hrpf = -8561991.6;
Hrpco2 = 282800;
HV = (-Hrpf*1000)/Mfuel;
```

Diffuser Calculations

```
To1 = Ta*(1+((gamair-1)/2)*Ma^2);
Toa = To1;
Po1 = Pa*((1+(eta_diff*((gamair-1)/2)*Ma^2))^(gamair/(gamair-1)));


for j = 1:length(compLow)
```

Compressor Calculations

```
    %Low Pressure Compressor Calculations
        Po2(j) = Po1*compLow(j);
        To2(j) = To1 + ((To1*((((compLow(j)^((gamair-1)/gamair))-1)))/eta_comp));
        wclp(j) = Cpoa*(To1-To2(j));

    %High Pressure Compressor Calculations
        Po3(j) = Po2(j)*compHigh(j);
        To3(j) = To2(j) + ((To2(j)*((((compHigh(j)^((gamair-1)/gamair))-1)))/eta_comp));
        wchp(j) = Cpoa*(To2(j)-To3(j));

    %Temperatures
        Tr(j) = To3(j);
        Tint = 1922;
        Tp = Tint;
```

Combustion Chamber Calculations

```
    Po4(j) = (1-delta_burn)*Po3(j);
    To4 = Tint;

%Delta h Caclulation
    hTr = A(:,1) + B(:,1)*Tr(j) + C(:,1)*log(Tr(j));

    if Tp <= 1600
       hTp = A(:,1) + B(:,1)*Tp + C(:,1)*log(Tp);
    elseif Tp > 1600
       hTp = A(:,2) + B(:,2)*Tp + C(:,2)*log(Tp);
    end

    delta_h = hTp - hTr;
    y(j) = (-Hrpf - MC*delta_h(2) - (MH/2)*delta_h(3) + ycc*delta_h(4))/(delta_h(4) + 3.76*delta_h(5));


%f calculation
    fideal(j) = (1/(4.76*y(j)))*(Mfuel/Mair);
    fact(j) = fideal(j)/eta_burn;
```

Turbine Calculations

```
          %High Pressure Turbine Calculations
    To5(j) = To4 + (wchp(j)/(eta_mech*(1+fact(j))*Cpog));
    Po5(j) = Po4(j)*(1-(((1-(To5(j)/To4))/eta_turb)))^(gamgas/(gamgas-1));

          %Low Pressure Turbine Calculations
    To6(j) = To5(j) + (wclp(j)/(eta_mech*(1+fact(j))*Cpog));
    Po6(j) = Po5(j)*(1-(((1-(To6(j)/To5(j)))/eta_turb)))^(gamgas/(gamgas-1));

    Pstar_overPo6 = (1-((1/eta_nozz)*(1-(2/(gamgas+1)))))^(gamgas/(gamgas-1));
    Pa_overPo6(j) = Pa/Po6(j);
```

Nozzle Calculations

```
          %Choke Test
    if Pa_overPo6(j) <= Pstar_overPo6
       Me = 1;
       Pe(j) = Po6(j)*Pstar_overPo6;
       Te(j) = To6(j)*(2/(gamgas+1));
       rho_exit(j) = Pe(j)/(Rgas*Te(j)/1000);
       Ve(j) = Me*sqrt(gamgas*Rgas*Te(j));
    else
       Pe(j) = Pa;
```

```
    Te(j) = To6(j)*(1-(eta_nozz*(1-((Pe(j)/Po6(j))^((gamgas-1)/gamgas)))));
    rho_exit(j) = Pe(j)/(Rgas*Te(j)/1000);
    Me(j) = sqrt(((To6(j)/Te(j))-1)*(2/(gamgas-1)));
    Ve(j) = Me(j)*sqrt(gamgas*Rgas*Te(j));
end
```

Specific Thrust & Fuel Consumption Calculations

```
Fs(j) = (((1+fact(j)))*Ve(j))-Va + (1000*(Pe(j)-Pa))*((1+fact(j))/(rho_exit(j)*Ve(j)));
tsfc(j) = (fact(j)/Fs(j))*3600;
```

Efficiencies

```
energy(j) = ((((1+fact(j))*((Ve(j)^2)/2)))-((Va^2)/2));
pressure(j) = ((1000*(Pe(j)-Pa))*((1+fact(j))/(rho_exit(j)*Ve(j))))^2;
thermal_eff(j) = (pressure(j)+energy(j))/(fact(j)*HV);
propul_eff(j) = (Fs(j)*Va)/(energy(j)+pressure(j));
overall_eff(j) = propul_eff(j)*thermal_eff(j);
```

```
end
```

Appendix B: MATLAB Code for Turbojet with Afterburning

```
% Turbojet with Afterburning
clc, clear, close all
format longG

%Flight Conditons
Ma = 0.84;
Pa = 54.05;
Ta = 255.7;
OPR = 50;
compLow = [7,7,7,7,7,7,7,7,7,6.7,6.2,5.9,5.6,5.3];
compHigh = OPR./compLow;
Rair = 287;
Rgas = Rair;
gamair = 1.4;
gamgas = 1.3333;
Va = Ma*sqrt(gamair*Rair*Ta);
Cpoa = (gamair*Rair)/(gamair-1);
Cpog = (gamgas*Rgas)/(gamgas-1);

%Efficiencies
eta_diff = 0.93;
eta_comp = 0.87;
eta_burn = 0.98;
delta_burn = 0.04;
eta_mech = 0.99;
eta_turb = 0.9;
eta_nozz = 0.95;

%Molecular Weights
Mfuel = 197.7;
Mair = 28.97;
```

```
MC = 14.4;
MH = 24.9;
MO = 0;
ycc = MC + (MH/4) - (MO/2);

%Delta h Constants
A = [299180, 309070;
   56835, 93048;
   88923, 154670;
   43388, 127010;
   31317, 44639];

B = [37.85, 39.29;
   66.27, 68.58;
   49.36, 60.43;
   42.27, 46.25;
   37.46, 39.32];

C = [-4571.9, -6201.9;
   -11634, -16979;
   -7940.8, -19212;
   -6635.4, -18798;
   -4559.3, -6753.4];

%Other Constants
Hrpf = -8561991.6;
Hrpco2 = 282800;
HV = (-Hrpf*1000)/Mfuel;
```

Diffuser Calculations

```
   To1 = Ta*(1+((gamair-1)/2)*Ma^2);
   Toa = To1;
   Po1 = Pa*((1+(eta_diff*((gamair-1)/2)*Ma^2))^(gamair/(gamair-1)));

for i = 1:length(compLow)
```

Compressor Calculations

```
   %Low Pressure Compressor Calculations
      Po2(i) = Po1*compLow(i);
      To2(i) = To1 + ((To1*((((compLow(i)^((gamair-1)/gamair))-1)))/eta_comp));
      wclp(i) = Cpoa*(To1-To2(i));

   %High Pressure Compressor Calculations
      Po3(i) = Po2(i)*compHigh(i);
```

```
    To3(i) = To2(i) + ((To2(i)*((((compHigh(i)^((gamair-1)/gamair))-1)))/eta_comp));
    wchp(i) = Cpoa*(To2(i)-To3(i));

%Temperatures
    Tr(i) = To3(i);
    Tint = 1922;
    Tp = Tint;
```

Primary Combustion Chamber Calculations

```
    Po4(i) = (1-delta_burn)*Po3(i);
    To4 = Tint;
    hTr = A(:,1) + B(:,1)*Tr(i) + C(:,1)*log(Tr(i));

%Delta h Caclulation
    if Tp <= 1600
       hTp = A(:,1) + B(:,1)*Tp + C(:,1)*log(Tp);
    elseif Tp > 1600
       hTp = A(:,2) + B(:,2)*Tp + C(:,2)*log(Tp);
    end

    delta_h = hTp - hTr;
    y(i) = (-Hrpf - MC*delta_h(2) - (MH/2)*delta_h(3) + ycc*delta_h(4))/(delta_h(4) + 3.76*delta_h(5));

%f calculation
    fideal(i) = (1/(4.76*y(i)))*(Mfuel/Mair);
    fact(i) = fideal(i)/eta_burn;
```

Turbine Calculations

```
%High Pressure Turbine Calculations
    To5(i) = To4 + (wchp(i)/(eta_mech*(1+fact(i))*Cpog));
    Po5(i) = Po4(i)*(1-(((1-(To5(i)/To4))/eta_turb)))^(gamgas/(gamgas-1));

%Low Pressure Turbine Calculations
    To6(i) = To5(i) + (wclp(i)/(eta_mech*(1+fact(i))*Cpog));
    Po6(i) = Po5(i)*(1-(((1-(To6(i)/To5(i)))/eta_turb)))^(gamgas/(gamgas-1));
```

Afterburner Calculations

```
%Temperatures
    Trab(i) = To6(i);
    Tpab = 2516;
    To7 = Tpab;
    hTrab = A(:,1) + B(:,1)*Trab + C(:,1)*log(Trab);
```

```
        %Afterburner Combustion Delta h Calculation
    if Tpab <= 1600
       hTpab = A(:,1) + B(:,1)*Tpab + C(:,1)*log(Tpab);
    elseif Tpab > 1600
       hTpab = A(:,2) + B(:,2)*Tpab + C(:,2)*log(Tpab);
    end

    delta_hab = hTpab - hTrab;

    x(i) = 1/y(i);
    z(i) = ((((3.76*delta_hab(5)+delta_hab(4))+(x(i)*(((MC*delta_hab(2))+((MH/2)*delta_hab(3))-(ycc*delta_hab(4))))))/((-Hrpf)-
(MC*delta_hab(2))-((MH/2)*delta_hab(3))+(ycc*delta_hab(4))));
    fo(i) = ((x(i)/eta_burn)+(z(i)/eta_burn))*(Mfuel/(4.76*Mair));

    Po7(i) = Po6(i)*(1-delta_burn);

    Pstar_overPo7 = (1-((1/eta_nozz)*(1-(2/(gamgas+1)))))^(gamgas/(gamgas-1));
    Pa_overPo7(i) = Pa/Po7(i);
```

Nozzle Calculations

```
  %Choke Test
    if Pa_overPo7(i) <= Pstar_overPo7
       Me = 1;
       Pe(i) = Po7(i)*Pstar_overPo7;
       Te(i) = To7*(2/(gamgas+1));
       rho_exit(i) = Pe(i)/(Rgas*Te(i)/1000);
       Ve(i) = Me*sqrt(gamgas*Rgas*Te(i));
    else
       Pe(i) = Pa;
       Te(i) = To7*(1-(eta_nozz*(1-((Pe(i)/Po7(i))^((gamgas-1)/gamgas)))));
       rho_exit(i) = Pe(i)/(Rgas*Te(i)/1000);
       Me(i) = sqrt(((To7/Te(i))-1)*(2/(gamgas-1)));
       Ve(i) = Me(i)*sqrt(gamgas*Rgas*Te(i));
    end
```

Specific Thrust & Fuel Consumption Calculations

```
    Fs(i) = (((1+fo(i)))*Ve(i))-Va + (1000*(Pe(i)-Pa))*((1+fo(i))/(rho_exit(i)*Ve(i)));
    tsfc(i) = (fo(i)/Fs(i))*3600;
```

Efficiencies

```
    energy(i) = ((((1+fo(i))*((Ve(i)^2)/2)))-((Va^2)/2));
    pressure(i) = ((1000*(Pe(i)-Pa))*((1+fo(i))/(rho_exit(i)*Ve(i))))^2;
    thermal_eff(i) = (pressure(i)+energy(i))/(fo(i)*HV);
```

```
        propul_eff(i) = (Fs(i)*Va)/(energy(i)+pressure(i));
        overall_eff(i) = propul_eff(i)*thermal_eff(i);
end
```

Appendix C: MATLAB Code for Turbofan

```
%Turbofan Engine, No mixing, No auxiliary burning (confirmed twice)
clc, clear, clear all
format longG
tic
%Flight Conditons
Ma = 0.84;
Ta = 255.7;
Pa = 54.05;
OPR = 50;
compLow = 1.3:0.1:(sqrt(OPR));
compHigh = OPR./compLow;
Rair = 287;
Rgas = Rair;
gamair = 1.4;
gamgas = 1.3333;
```

```
a = sqrt(gamair*Rair*Ta);
Va = Ma*a;
Cpoa = (gamair*Rair)/(gamair-1);
Cpog = (gamgas*Rgas)/(gamgas-1);
Cpox = 1241;
b = 1.5;

%Efficiencies
eta_diff = .93;
eta_comp = .87;
eta_burn = .98;
delta_burn = 0.04;
eta_mech = .99;
eta_turb = .9;
eta_nozz = 0.95;

%Molecular Weights
Mfuel = 197.7;
Mair = 28.97;
MC = 14.4;
MH = 24.9;
MO = 0;
ycc = MC + (MH/4) - (MO/2);

%Delta h Constants
A = [299180, 309070;
   56835, 93048;
   88923, 154670;
   43388, 127010;
   31317, 44639];

B = [37.85, 39.29;
   66.27, 68.58;
   49.36, 60.43;
   42.27, 46.25;
   37.46, 39.32];

C = [-4571.9, -6201.9;
   -11634, -16979;
   -7940.8, -19212;
   -6635.4, -18798;
   -4559.3, -6753.4];


%Other Constants
Hrpf = -8561991.6;
```

```
Hrpco2 = 282800;
HV = (-Hrpf*1000)/Mfuel;
```

Diffuser Calculations

```
To1 = Ta*(1+((gamair-1)/2)*(Ma^2));
Toa = To1;
Po1 = Pa*((1+(eta_diff*((gamair-1)/2)*(Ma^2))).^(gamair/(gamair-1)));


for j = 1:length(compLow)
```

Compressor Calculations

```
        %Low Pressure Compressor Calculations
    Po2(j) = Po1*compLow(j);
    To2(j) = To1 + ((To1*((((compLow(j)^((gamair-1)/gamair))-1)))/eta_comp));
    wclp(j) = Cpoa*(To1-To2(j))*(b+1);
    Pstar_overPo2 = (1-((1/eta_nozz)*(1-(2/(gamair+1)))))^(gamair/(gamair-1));
    Pa_overPo2(j) = Pa/Po2(j);

        %High Pressure Compressor Calculations
    Po3(j) = Po2(j)*compHigh(j);
    To3(j) = To2(j) + ((To2(j)*((((compHigh(j)^((gamair-1)/gamair))-1)))/eta_comp));
    wchp(j) = Cpoa*(To2(j)-To3(j));

        %Temperatures
    Trbp(j) = To2(j);
    Tr(j) = To3(j);
    Tint = 1922;
    Tp = Tint;
```

Combustion Chamber Calculations

```
    Po4(j) = (1-delta_burn)*Po3(j);
    To4 = Tint;
    hTr = A(:,1) + B(:,1)*Tr(j) + C(:,1)*log(Tr(j));

        %Delta h Caclulation
    if Tp <= 1600
       hTp = A(:,1) + B(:,1)*Tp + C(:,1)*log(Tp);
    elseif Tp > 1600
       hTp = A(:,2) + B(:,2)*Tp + C(:,2)*log(Tp);
    end

    delta_h = hTp - hTr;
```

```
y(j) = (-Hrpf - MC*delta_h(2) - (MH/2)*delta_h(3) + ycc*delta_h(4))/(delta_h(4) + 3.76*delta_h(5));

        %f calculation
fideal(j) = (1/(4.76*y(j)))*(Mfuel/Mair);
fact(j) = fideal(j)/eta_burn;
fo(j) = fact(j)/(b+1);
```

Turbine Calculations

```
        %High Pressure Turbine Calculations
To5(j) = To4 + (wchp(j)/(eta_mech*(1+fact(j))*Cpog));
Po5(j) = Po4(j)*(1-(((1-(To5(j)/To4))/eta_turb)))^(gamgas/(gamgas-1));

        %Low Pressure Turbine Calculations
To6(j) = To5(j) + (wclp(j)/(eta_mech*(1+fact(j))*Cpog));
Po6(j) = Po5(j)*(1-(((1-(To6(j)/To5(j)))/eta_turb)))^(gamgas/(gamgas-1));
Pstar_overPo6 = (1-((1/eta_nozz)*(1-(2/(gamgas+1)))))^(gamgas/(gamgas-1));
Pa_overPo6(j) = Pa/Po6(j);
```

Nozzle Calculations

```
        %Cold Nozzle Choke Test
if Pa_overPo2(j) <= Pstar_overPo2
   Mec(j) = 1;
   Pec(j) = Po2(j)*Pstar_overPo2;
   Tec(j) = To2(j)*(2/(gamair+1));
   rho_exitc(j) = Pec(j)/(Rair*Tec(j)/1000);
   Vec(j) = Mec(j)*sqrt(gamair*Rair*Tec(j));
else
   Pec(j) = Pa;
   Tec(j) = To6(j)*(1-(eta_nozz*(1-(((Pec(j)/Po2(j)))^((gamair-1)/gamair)))));
   rho_exitc(j) = Pec(j)/(Rair*Tec(j)/1000);
   Mec(j) = sqrt(((To2(j)/Tec(j))-1)*(2/(gamair-1)));
   Vec(j) = Mec(j)*sqrt(gamair*Rair*Tec(j));
end

        %Hot Nozzle Choke Test
if Pa_overPo6(j) <= Pstar_overPo6
   Me = 1;
   Pe(j) = Po6(j)*Pstar_overPo6;
   Te(j) = To6(j)*(2/(gamgas+1));
   rho_exit(j) = Pe(j)/(Rgas*Te(j)/1000);
   Ve(j) = Me*sqrt(gamgas*Rgas*Te(j));
else
   Pe(j) = Pa;
   Te(j) = To6(j)*(1-(eta_nozz*(1-(((Pe(j)/Po6(j)))^((gamgas-1)/gamgas)))));
```

```
        rho_exit(j) = Pe(j)/(Rgas*Te(j)/1000);
        Me(j) = sqrt(((To6(j)/Te(j))-1)*(2/(gamgas-1)));
        Ve(j) = Me(j)*sqrt(gamgas*Rgas*Te(j));
    end
```

Specific Thrust & Fuel Consumption Calculations

```
    Fs(j) = (1/(b+1))*((((1+fact(j)))*Ve(j))-Va + (1000*(Pe(j)-Pa))*((1+fact(j))/(rho_exit(j)*Ve(j))))+((b/(b+1))*((Vec(j)-Va)+((1000*(Pec(j)-Pa))*(1/(rho_exitc(j)*Vec(j))))));
    tsfc(j) = (fo(j)/Fs(j))*3600;
```

Efficiencies

```
    energy_hot(j) = (1/(b+1))*((((1+fact(j))*((Ve(j)^2)/2)))-((Va^2)/2));
    energy_cold(j) = (b/(b+1))*((((Vec(j)^2)/2)-((Va^2)/2)));
    energy(j) = energy_hot(j) + energy_cold(j);
    pressure_hot(j) = (1/(b+1))*(((1000*(Pe(j)-Pa))*((1+fact(j))/(rho_exit(j)*Ve(j))))^2);
    pressure_cold(j) = (b/(b+1))*(((1000*(Pec(j)-Pa))*(1/(rho_exitc(j)*Vec(j))))^2);
    pressure(j) = pressure_hot(j) + pressure_cold(j);
    thermal_eff(j) = (pressure(j)+energy(j))/(fo(j)*HV);
    propul_eff(j) = (Fs(j)*Va)/(energy(j)+pressure(j));
    overall_eff(j) = propul_eff(j)*thermal_eff(j);
```

```
end


[mint,p1] = min(tsfc);
optFPRt = compLow(p1);

[maxF,p2] = max(Fs);
optFPRF = compLow(p2);

table = [optFPRt' mint' optFPRF' maxF'];

eff_overall = 100*Va./(tsfc*-Hrpf);


toc
```

Appendix D: MATLAB Code for Turbofan with Mixing

```
%Turbofan Engine, No Auxiliary burning w/mixing (confirmed twice)
clc, clear, close all
format longG
tic
%Flight Conditons
Ma = 0.84;
Ta = 255.7;
Pa = 54.05;
OPR = 50;
compLow = [7,7,7,7,7,7,7,7,7,7,6.7,6.2,5.9,5.6,5.3];
compHigh = OPR./compLow;
Rair = 287;
Rgas = Rair;
gamair = 1.4;
gamgas = 1.3333;
a = sqrt(gamair*Rair*Ta);
Va = Ma*a;
Cpoa = (gamair*Rair)/(gamair-1);
Cpog = (gamgas*Rgas)/(gamgas-1);
Cpox = 1241;
k = (gamair/gamgas)*((gamgas-1)/(gamair-1));
b = 0.1:0.1:1.5;


%Efficiencies
eta_diff = .93;
eta_comp = .87;
eta_burn = .98;
delta_burn = 0.04;
delta_chute = 0.02;
eta_mech = .99;
eta_turb = .9;
eta_nozz = 0.95;

%Molecular Weights
Mfuel = 197.7;
Mair = 28.97;
MC = 14.4;
MH = 24.9;
MO = 0;
ycc = MC + (MH/4) - (MO/2);

%Delta h Constants
A = [299180, 309070;
```

```
    56835, 93048;
    88923, 154670;
    43388, 127010;
    31317, 44639];

B = [37.85, 39.29;
    66.27, 68.58;
    49.36, 60.43;
    42.27, 46.25;
    37.46, 39.32];

C = [-4571.9, -6201.9;
    -11634, -16979;
    -7940.8, -19212;
    -6635.4, -18798;
    -4559.3, -6753.4];


%Other Constants
Hrpf = -8561991.6;
HV = (-Hrpf*1000)/Mfuel;
Hrpco2 = 282800;
Fs = zeros(1,15);
tsfc = zeros(1,15);
```

Diffuser Calculations

```
To1 = Ta*(1+((gamair-1)/2)*(Ma^2));
Toa = To1;
Po1 = Pa*((1+(eta_diff*((gamair-1)/2)*(Ma^2))).^(gamair/(gamair-1)));

for i = 1:length(b)
```

Compressor Calculations

```
        %Low Pressure Compressor Calculations
    Po2(i) = Po1*compLow(i);
    To2(i) = To1 + ((To1*((((compLow(i)^((gamair-1)/gamair))-1)))/eta_comp));
    wclp(i) = Cpoa*(To1-To2(i))*(b(i)+1);

        %High Pressure Compressor Calculations
    Po3(i) = Po2(i)*compHigh(i);
    To3(i) = To2(i) + ((To2(i)*((((compHigh(i)^((gamair-1)/gamair))-1)))/eta_comp));
    wchp(i) = Cpoa*(To2(i)-To3(i));

        %Temperatures
```

```
Trbp(i) = To2(i);
Tr(i) = To3(i);
Tint = 1922;
Tp = Tint;
```

Combustion Chamber Calculations

```
Po4(i) = (1-delta_burn)*Po3(i);
To4 = Tint;
hTr = A(:,1) + B(:,1)*Tr(i) + C(:,1)*log(Tr(i));

        %Delta h Caclulation
if Tp <= 1600
   hTp = A(:,1) + B(:,1)*Tp + C(:,1)*log(Tp);
elseif Tp > 1600
   hTp = A(:,2) + B(:,2)*Tp + C(:,2)*log(Tp);
end

delta_h = hTp - hTr;
y(i) = (-Hrpf - MC*delta_h(2) - (MH/2)*delta_h(3) + ycc*delta_h(4))/(delta_h(4) + 3.76*delta_h(5));

        %f calculation
fideal(i) = (1/(4.76*y(i)))*(Mfuel/Mair);
fact(i) = fideal(i)/eta_burn;
fo(i) = fact(i)/(b(i)+1);
```

Turbine Calculations

```
%High Pressure Turbine Calculations
   To5(i) = To4 + (wchp(i)/(eta_mech*(1+fact(i))*Cpog));
   Po5(i) = Po4(i)*(1-(((1-(To5(i)/To4))/eta_turb)))^(gamgas/(gamgas-1));

%Low Pressure Turbine Calculations
   To6(i) = To5(i) + (wclp(i)/(eta_mech*(1+fact(i))*Cpog));
   Po6(i) = Po5(i)*(1-(((1-(To6(i)/To5(i)))/eta_turb)))^(gamgas/(gamgas-1));
```

Stream Mixing Calculations

```
To8(i) = Trbp(i);
Po8(i) = Po2(i)*(1-delta_chute);
To7(i) = ((To8(i)*k*b(i))+(To6(i)*(1+fact(i))))/(1+fact(i)+(k*b(i)));
Po7(i) = ((Po8(i)*b(i))+(Po6(i)*(1+fact(i))))/(1+b(i)+fact(i));
Pstar_overPo7 = (1-((1/eta_nozz)*(1-(2/(gamgas+1)))))^(gamgas/(gamgas-1));
Pa_overPo7(i) = Pa/Po7(i);
```

Nozzle Calculations

```
%Nozzle Choke Test
    if Pa_overPo7(i) <= Pstar_overPo7
        Me = 1;
        Pe(i) = Po7(i)*Pstar_overPo7;
        Te(i) = To7(i)*(2/(gamgas+1));
        rho_exit(i) = Pe(i)/(Rgas*Te(i)/1000);
        Ve(i) = Me*sqrt(gamgas*Rgas*Te(i));
    else
        Pe(i) = Pa;
        Te(i) = To7(i)*(1-(eta_nozz*(1-(((Pe(i)/Po7(i)))^((gamgas-1)/gamgas)))));
        rho_exit(i) = Pe(i)/(Rgas*Te(i)/1000);
        Me(i) = sqrt(((To7(i)/Te(i))-1)*(2/(gamgas-1)));
        Ve(i) = Me(i)*sqrt(gamgas*Rgas*Te(i));
    end
```

Specific Thrust & Fuel Consumption Calculations

```
    Fs(i) = ((((1+fo(i)))*Ve(i))-Va + (1000*(Pe(i)-Pa))*((1+fo(i))/(rho_exit(i)*Ve(i))));
    tsfc(i) = (fo(i)/Fs(i))*3600;
```

Efficiencies

```
    energy(i) = ((((1+fo(i))*((Ve(i)^2)/2)))-((Va^2)/2));
    pressure(i) = ((1000*(Pe(i)-Pa))*((1+fo(i))/(rho_exit(i)*Ve(i))))^2;
    thermal_eff(i) = (pressure(i)+energy(i))/(fo(i)*HV);
    propul_eff(i) = (Fs(i)*Va)/(energy(i)+pressure(i));
    overall_eff(i) = propul_eff(i)*thermal_eff(i);
```

```
end


toc
```

Appendix E: MATLAB Code for Turbofan with Mixing and Afterburning

```
% Turbofan with Afterburner (confirmed twice)
clc, clear, close all
format longG

%Flight Conditons
Ma = 0.84;
Pa = 54.05;
Ta = 255.7;
OPR = 50;
compLow = [7,7,7,7,7,7,7,7,7,7,6.7,6.2,5.9,5.6,5.3];
compHigh = OPR./compLow;
Rair = 287;
Rgas = Rair;
gamair = 1.4;
gamgas = 1.3333;
Va = Ma*sqrt(gamair*Rair*Ta);
Cpoa = (gamair*Rair)/(gamair-1);
Cpog = (gamgas*Rgas)/(gamgas-1);
k = (gamair/gamgas)*((gamgas-1)/(gamair-1));
b = 0.1:0.1:1.5;


%Efficiencies
eta_diff = 0.93;
eta_comp = 0.87;
eta_burn = 0.98;
delta_burn = 0.04;
delta_chute = 0.02;
eta_mech = 0.99;
eta_turb = 0.9;
```

```
eta_nozz = 0.95;

%Molecular Weights
Mfuel = 197.7;
Mair = 28.97;
MC = 14.4;
MH = 24.9;
MO = 0;
ycc = MC + (MH/4) - (MO/2);


%Other Constants
Hrpf = -8561991.6;
Hrpco2 = 282800;
HV = (-Hrpf*1000)/Mfuel;
Fs = zeros(1,15);
tsfc = zeros(1,15);
% Fnoab = 535.841;
% tnoab = 0.112984;


%Delta h Constants
A = [299180, 309070;
   56835, 93048;
   88923, 154670;
   43388, 127010;
   31317, 44639];

B = [37.85, 39.29;
   66.27, 68.58;
   49.36, 60.43;
   42.27, 46.25;
   37.46, 39.32];

C = [-4571.9, -6201.9;
   -11634, -16979;
   -7940.8, -19212;
   -6635.4, -18798;
   -4559.3, -6753.4];


for i = 1:length(b)
```

Diffuser Calculations

```
To1 = Ta*(1+((gamair-1)/2)*(Ma^2));
Toa = To1;
Po1 = Pa*((1+(eta_diff*((gamair-1)/2)*Ma^2))^(gamair/(gamair-1)));
```

Compressor Calculations

```
%Low Pressure Compressor Calculations
   Po2(i) = Po1*compLow(i);
   To2(i) = To1 + ((To1*((((compLow(i)^((gamair-1)/gamair))-1)))/eta_comp));
   wclp(i) = Cpoa*(To1-To2(i))*(b(i)+1);

         %High Pressure Compressor Calculations
   Po3(i) = Po2(i)*compHigh(i);
   To3(i) = To2(i) + ((To2(i)*((((compHigh(i)^((gamair-1)/gamair))-1)))/eta_comp));
   wchp(i) = Cpoa*(To2(i)-To3(i));

%Temperatures
   Tr(i) = To3(i);
   Tint = 1922;
   Tp = Tint;
```

Primary Combustion Chamber Calculations

```
Po4(i) = (1-delta_burn)*Po3(i);
To4 = Tint;
hTr = A(:,1) + B(:,1)*Tr(i) + C(:,1)*log(Tr(i));

%Delta h Caclulation
   if Tp <= 1600
      hTp = A(:,1) + B(:,1)*Tp + C(:,1)*log(Tp);
   elseif Tp > 1600
      hTp = A(:,2) + B(:,2)*Tp + C(:,2)*log(Tp);
   end

   delta_h = hTp - hTr;
   y(i) = (-Hrpf - MC*delta_h(2) - (MH/2)*delta_h(3) + ycc*delta_h(4))/(delta_h(4) + 3.76*delta_h(5));
   x(i) = 1/y(i);

%f calculation
   fideal(i) = (1/(4.76*y(i)))*(Mfuel/Mair);
   fact(i) = fideal(i)/eta_burn;
```

Turbine Calculations

```
%High Pressure Turbine Calculations
    To5(i) = To4 + (wchp(i)/(eta_mech*(1+fact(i))*Cpog));
    Po5(i) = Po4(i)*(1-(((1-(To5(i)/To4))/eta_turb)))^(gamgas/(gamgas-1));

%Low Pressure Turbine Calculations
    To6(i) = To5(i) + (wclp(i)/(eta_mech*(1+fact(i))*Cpog));
    Po6(i) = Po5(i)*(1-(((1-(To6(i)/To5(i)))/eta_turb)))^(gamgas/(gamgas-1));
```

Stream Mixing Calculations

```
    To8 = To2(i);
    Po8(i) = Po2(i)*(1-delta_chute);
    To7(i) = ((To8*k*b(i))+(To6(i)*(1+fact(i))))/(1+fact(i)+(k*b(i)));
    Po7(i) = ((Po8(i)*b(i))+(Po6(i)*(1+fact(i))))/(1+b(i)+fact(i));
%       Pstar_overPo7 = (1-((1/eta_nozz)*(1-(2/(gamgas+1)))))^(gamgas/(gamgas-1));
%       Pa_overPo7 = Pa/Po7;
```

Afterburner Calculations

```
%Temperatures
    Trab(i) = To7(i);
    Tpab = 2516;
    To9 = Tpab;
    hTrab = A(:,1) + B(:,1)*Trab(i) + C(:,1)*log(Trab(i));

%Afterburner Combustion Delta h Calculation
    if Tpab <= 1600
       hTpab = A(:,1) + B(:,1)*Tpab + C(:,1)*log(Tpab);
    elseif Tpab > 1600
       hTpab = A(:,2) + B(:,2)*Tpab + C(:,2)*log(Tpab);
    end

    delta_hab = hTpab - hTrab;

    xo(i) = (1/y(i))/(b(i)+1);
    z(i) = ((((3.76*delta_hab(5))+delta_hab(4))+(xo(i)*(((MC*delta_hab(2))+((MH/2)*delta_hab(3))-(ycc*delta_hab(4))))))/((-Hrpf)-
(MC*delta_hab(2))-((MH/2)*delta_hab(3))+(ycc*delta_hab(4))));
    fo(i) = ((xo(i)/eta_burn)+(z(i)/eta_burn))*(Mfuel/(4.76*Mair));

    Po9(i) = Po7(i)*(1-delta_burn);

    Pstar_overPo9 = (1-((1/eta_nozz)*(1-(2/(gamgas+1)))))^(gamgas/(gamgas-1));
    Pa_overPo9(i) = Pa/Po9(i);
```

Nozzle Calculations

```
%Nozzle Choke Test
    if Pa_overPo9(i) <= Pstar_overPo9
        Me = 1;
        Pe(i) = Po9(i)*Pstar_overPo9;
        Te(i) = To9*(2/(gamgas+1));
        rho_exit(i) = Pe(i)/(Rgas*Te(i)/1000);
        Ve(i) = Me*sqrt(gamgas*Rgas*Te(i));
    else
        Pe(i) = Pa;
        Te(i) = To9*(1-(eta_nozz*(1-((Pe(i)/Po9(i))^((gamgas-1)/gamgas)))));
        rho_exit(i) = Pe(i)/(Rgas*Te(i)/1000);
        Me(i) = sqrt(((To9/Te(i))-1)*(2/(gamgas-1)));
        Ve(i) = Me*sqrt(gamgas*Rgas*Te(i));
    end
```

Specific Thrust & Fuel Consumption Calculations

```
    Fs(i) = (((1+fo(i)))*Ve(i))-Va + (1000*(Pe(i)-Pa))*((1+fo(i))/(rho_exit(i)*Ve(i)));
    tsfc(i) = (fo(i)/Fs(i))*3600;
```

Efficiencies

```
    energy(i) = ((((1+fo(i))*((Ve(i)^2)/2)))-((Va^2)/2));
    pressure(i) = ((1000*(Pe(i)-Pa))*((1+fo(i))/(rho_exit(i)*Ve(i))))^2;
    thermal_eff(i) = (pressure(i)+energy(i))/(fo(i)*HV);
    propul_eff(i) = (Fs(i)*Va)/(energy(i)+pressure(i));
    overall_eff(i) = propul_eff(i)*thermal_eff(i);
end
```

Appendix F: MATLAB Code for TurboAux

```
%Turbofan Engine, Auxiliary burning w/mixing (confirmed twice)
clc, clear all, close all
format longG
tic
%Flight Conditons
Ma = 0.84;
Ta = 255.7;
Pa = 54.05;
OPR = 50;
```

```
compLow = [7,7,7,7,7,7,7,7,7,6.7,6.2,5.9,5.6,5.3];
compHigh = OPR./compLow;
Rair = 287;
Rgas = Rair;
gamair = 1.4;
gamgas = 1.3333;
a = sqrt(gamair*Rair*Ta);
Va = Ma*a;
Cpoa = (gamair*Rair)/(gamair-1);
Cpog = (gamgas*Rgas)/(gamgas-1);
Cpox = 1241;
b = 0.1:0.1:1.5;


%Efficiencies
eta_diff = .93;
eta_comp = .87;
eta_burn = .98;
delta_burn = 0.04;
eta_mech = .99;
eta_turb = .9;
eta_nozz = 0.95;

%Molecular Weights
Mfuel = 197.7;
Mair = 28.97;
MC = 14.4;
MH = 24.9;
MO = 0;
ycc = MC + (MH/4) - (MO/2);

%Delta h Constants
A = [299180, 309070;
   56835, 93048;
   88923, 154670;
   43388, 127010;
   31317, 44639];

B = [37.85, 39.29;
   66.27, 68.58;
   49.36, 60.43;
   42.27, 46.25;
   37.46, 39.32];

C = [-4571.9, -6201.9;
   -11634, -16979;
```

```
    -7940.8, -19212;
    -6635.4, -18798;
    -4559.3, -6753.4];


%Other Constants
Hrpf = -8561991.6;
HV = (-Hrpf*1000)/Mfuel;
Hrpco2 = 282800;
Fs = zeros(1,15);
tsfc = zeros(1,15);
```

Diffuser Calculations

```
To1 = Ta*(1+((gamair-1)/2)*(Ma^2));
Toa = To1;
Po1 = Pa*((1+(eta_diff*((gamair-1)/2)*(Ma^2))).^(gamair/(gamair-1)));

for i = 1:length(b)
```

Compressor Calculations

```
        %Low Pressure Compressor Calculations
    Po2(i) = Po1*compLow(i);
    To2(i) = To1 + ((To1*((((compLow(i)^((gamair-1)/gamair))-1)))/eta_comp));
    wclp(i) = Cpoa*(To1-To2(i))*(b(i)+1);

        %High Pressure Compressor Calculations
    Po3(i) = Po2(i)*compHigh(i);
    To3(i) = To2(i) + ((To2(i)*((((compHigh(i)^((gamair-1)/gamair))-1)))/eta_comp));
    wchp(i) = Cpoa*(To2(i)-To3(i));

        %Temperatures
    Trbp(i) = To2(i);
    Tr(i) = To3(i);
    Tint = 1922;
    Tp = Tint;
```

Primary Combustion Chamber Calculations

```
    Po4(i) = (1-delta_burn)*Po3(i);
    To4 = Tint;
    hTr = A(:,1) + B(:,1)*Tr(i) + C(:,1)*log(Tr(i));

        %Delta h Caclulation
    if Tp <= 1600
```

```
    hTp = A(:,1) + B(:,1)*Tp + C(:,1)*log(Tp);
elseif Tp > 1600
    hTp = A(:,2) + B(:,2)*Tp + C(:,2)*log(Tp);
end

delta_h = hTp - hTr;
y(i) = (-Hrpf - MC*delta_h(2) - (MH/2)*delta_h(3) + ycc*delta_h(4))/(delta_h(4) + 3.76*delta_h(5));

        %f calculation
fideal(i) = (1/(4.76*y(i)))*(Mfuel/Mair);
fact(i) = fideal(i)/eta_burn;
```

Auxiliary Combustion Chamber Calculations

```
Pbp(i) = Po2(i)*(1-delta_burn);
Tbp = 2516;
hTrbp = A(:,1) + B(:,1)*Trbp(i) + C(:,1)*log(Trbp(i));

        %Auxiliary Combustion Delta h Calculation
if Tbp <= 1600
    hTbp = A(:,1) + B(:,1)*Tbp + C(:,1)*log(Tbp);
elseif Tbp > 1600
    hTbp = A(:,2) + B(:,2)*Tbp + C(:,2)*log(Tbp);
end

dH = hTbp - hTrbp;
ybp(i) = (-Hrpf - MC*dH(2) - (MH/2)*dH(3) + ycc*dH(4))/(dH(4) + 3.76*dH(5));

%f calculation
    fib(i) = (1/(4.76*ybp(i)))*(Mfuel/Mair);
    fab(i) = fib(i)/eta_burn;
    fo(i) = ((b(i)*fab(i))/(b(i)+1))+((fact(i)/(b(i)+1)));
```

Turbine Calculations

```
%High Pressure Turbine Calculations
    To5(i) = To4 + (wchp(i)/(eta_mech*(1+fact(i))*Cpog));
    Po5(i) = Po4(i)*(1-(((1-(To5(i)/To4))/eta_turb)))^(gamgas/(gamgas-1));

%Low Pressure Turbine Calculations
    To6(i) = To5(i) + (wclp(i)/(eta_mech*(1+fact(i))*Cpog));
    Po6(i) = Po5(i)*(1-(((1-(To6(i)/To5(i)))/eta_turb)))^(gamgas/(gamgas-1));
```

Stream Mixing Calculations

```
    To8 = Tbp;
    Po8(i) = Pbp(i);
    To7(i) = ((To8*b(i)*(1+fab(i)))+(To6(i)*(1+fact(i))))/((1+fact(i))+(b(i)*(1+fab(i))));
    Po7(i) = ((Po8(i)*b(i)*(1+fab(i)))+(Po6(i)*(1+fact(i))))/((b(i)*(1+fab(i)))+(1+fact(i)));
    Pstar_overPo7 = (1-((1/eta_nozz)*(1-(2/(gamgas+1)))))^(gamgas/(gamgas-1));
    Pa_overPo7(i) = Pa/Po7(i);
```

Nozzle Calculations

```
%Nozzle Choke Test
    if Pa_overPo7(i) <= Pstar_overPo7
        Me = 1;
        Pe(i) = Po7(i)*Pstar_overPo7;
        Te(i) = To7(i)*(2/(gamgas+1));
        rho_exit(i) = Pe(i)/(Rgas*Te(i)/1000);
        Ve(i) = Me*sqrt(gamgas*Rgas*Te(i));
    else
        Pe(i) = Pa;
        Te(i) = To7(i)*(1-(eta_nozz*(1-(((Pe(i)/Po7(i)))^((gamgas-1)/gamgas)))));
        rho_exit(i) = Pe(i)/(Rgas*Te(i)/1000);
        Me(i) = sqrt(((To7(i)/Te(i))-1)*(2/(gamgas-1)));
        Ve(i) = Me(i)*sqrt(gamgas*Rgas*Te(i));
    end
```

Specific Thrust & Fuel Consumption Calculations

```
    Fs(i) = ((((1+fo(i)))*Ve(i))-Va + (1000*(Pe(i)-Pa))*((1+fo(i))/(rho_exit(i)*Ve(i))));
    tsfc(i) = (fo(i)/Fs(i))*3600;
```

Efficiencies

```
    energy(i) = ((((1+fo(i))*((Ve(i)^2)/2)))-((Va^2)/2));
    pressure(i) = ((1000*(Pe(i)-Pa))*((1+fo(i))/(rho_exit(i)*Ve(i))))^2;
    thermal_eff(i) = (pressure(i)+energy(i))/(fo(i)*HV);
    propul_eff(i) = (Fs(i)*Va)/(energy(i)+pressure(i));
    overall_eff(i) = propul_eff(i)*thermal_eff(i);
```

```
end


toc
```

Appendix G: Performance Results Tables

Table 24. Performance Results at BPR of 0.2

Engine	Turbojet with Afterburning	Turbofan with Afterburning	TurboAux
FPR	7	7	7
Bypass Ratio	N/A	0.2	0.2
Fs	1319.787153	1300.580112	896.058862
TSFC	0.1923519	0.195805488	0.1374408
Propulsive Efficiency	45.23%	45.95%	58.46%
Thermal Efficiency	25.72%	24.88%	27.86%
Overall Efficiency	11.64%	11.43%	16.28%

Table 25. Performance Results at BPR of 0.3

Engine	Turbojet with Afterburning	Turbofan with Afterburning	TurboAux

FPR	7	7	7
Bypass Ratio	N/A	0.3	0.3
Fs	1319.787153	1292.075745	918.0701803
TSFC	0.1923519	0.19747441	0.143614704
Propulsive Efficiency	45.23%	46.26%	57.69%
Thermal Efficiency	25.72%	24.50%	27.01%
Overall Efficiency	11.64%	11.33%	15.58%

Table 26. Performance Results at BPR of 0.4

Engine	Turbojet with Afterburning	Turbofan with Afterburning	TurboAux
FPR	7	7	7
Bypass Ratio	N/A	0.4	0.4
Fs	1319.787153	1284.348251	935.9424414
TSFC	0.1923519	0.199051338	0.148833687
Propulsive Efficiency	45.23%	46.55%	57.10%
Thermal Efficiency	25.72%	24.15%	26.33%
Overall Efficiency	11.64%	11.24%	15.04%

Table 27. Performance Results at BPR of 0.5

Engine	Turbojet with Afterburning	Turbofan with Afterburning	TurboAux
FPR	7	7	7
Bypass Ratio	N/A	0.5	0.5
Fs	1319.787153	1277.410785	950.770035
TSFC	0.1923519	0.200514892	0.153304825
Propulsive Efficiency	45.23%	46.81%	56.63%
Thermal Efficiency	25.72%	23.84%	25.78%
Overall Efficiency	11.64%	11.16%	14.60%

Table 28. Performance Results at BPR of 0.6

Engine	Turbojet with Afterburning	Turbofan with Afterburning	TurboAux
FPR	7	7	7
Bypass Ratio	N/A	0.6	0.6
Fs	1319.787153	1271.259589	963.3298799
TSFC	0.1923519	0.201853041	0.157171777
Propulsive Efficiency	45.23%	47.04%	56.24%
Thermal Efficiency	25.72%	23.57%	25.32%

Overall Efficiency	11.64%	11.09%	14.24%

Table 29. Performance Results at BPR of 0.7

Engine	Turbojet with Afterburning	Turbofan with Afterburning	TurboAux
FPR	7	7	7
Bypass Ratio	N/A	0.7	0.7
Fs	1319.787153	1265.875561	974.182386
TSFC	0.1923519	0.203060489	0.160538854
Propulsive Efficiency	45.23%	47.24%	55.91%
Thermal Efficiency	25.72%	23.33%	24.94%
Overall Efficiency	11.64%	11.02%	13.94%

Table 30. Performance Results at BPR of 0.9

Engine	Turbojet with Afterburning	Turbofan with Afterburning	TurboAux
FPR	7	7	7
Bypass Ratio	N/A	0.9	0.9
Fs	1319.787153	1257.271618	992.2910427
TSFC	0.1923519	0.205085379	0.166071592

Propulsive Efficiency	45.23%	47.56%	55.36%
Thermal Efficiency	25.72%	22.95%	24.34%
Overall Efficiency	11.64%	10.91%	13.48%

Table 31. Performance Results at BPR of 1.0

Engine	Turbojet with Afterburning	Turbofan with Afterburning	TurboAux
FPR	7	7	7
Bypass Ratio	N/A	1.0	1.0
Fs	1319.787153	1253.961329	1000.068212
TSFC	0.1923519	0.205911826	0.168348692
Propulsive Efficiency	45.23%	47.68%	55.13%
Thermal Efficiency	25.72%	22.79%	24.12%
Overall Efficiency	11.64%	10.87%	13.29%

Table 32. Performance Results at BPR of 1.1

Engine	Turbojet with Afterburning	Turbofan with Afterburning	TurboAux
FPR	6.7	6.7	6.7

Bypass Ratio	N/A	1.1	1.1
Fs	1319.769575	1247.544694	1005.445156
TSFC	0.192356365	0.207232666	0.171097707
Propulsive Efficiency	45.23%	47.92%	55.01%
Thermal Efficiency	25.72%	22.54%	23.78%
Overall Efficiency	11.64%	10.80%	13.08%

Table 33. Performance Results at BPR of 1.2

Engine	Turbojet with Afterburning	Turbofan with Afterburning	TurboAux
FPR	6.2	6.2	6.2
Bypass Ratio	N/A	1.2	1.2
Fs	1319.76	1238.022576	1008.311551
TSFC	0.192368	0.209067344	0.174330783
Propulsive Efficiency	45.23%	48.26%	55.02%
Thermal Efficiency	25.72%	22.18%	23.34%
Overall Efficiency	11.63%	10.71%	12.84%

Table 34. Performance Results at BPR of 1.3

Engine	Turbojet with Afterburning	Turbofan with Afterburning	TurboAux
FPR	5.9	5.9	5.9
Bypass Ratio	N/A	1.3	1.3
Fs	1319.768651	1230.590852	1011.313492
TSFC	0.192376785	0.210555501	0.177019723
Propulsive Efficiency	45.23%	48.53%	54.99%
Thermal Efficiency	25.72%	21.90%	22.99%
Overall Efficiency	11.63%	10.63%	12.64%

Table 35. Performance Results at BPR of 1.4

Engine	Turbojet with Afterburning	Turbofan with Afterburning	TurboAux
FPR	5.6	5.6	5.6
Bypass Ratio	N/A	1.4	1.4
Fs	1319.790155	1222.686224	1013.291988
TSFC	0.192388336	0.212125947	0.179700812
Propulsive Efficiency	45.23%	48.81%	55.00%
Thermal Efficiency	25.72%	21.62%	22.65%

Overall Efficiency	11.63%	10.55%	12.45%

VITA

Kaleab Fetahi is an Ethiopian-American born on March 26, 1996 in Addis Ababa. Kaleab and his family immigrated to the United States shortly after in October of 1996 and moved to Raleigh, NC where he was raised until the age of four. In late 1999, he and his family relocated to the suburbs of Washington D.C., in Northern Virginia. Growing up in Northern Virginia in the Fairfax County Public School system, he grew an affinity for science and mathematics and in his free time, when not outside, could be found reading children's encyclopedias. His life-long goal was to one day become an astronaut. In high school, he was a two-sport student-athlete competing for Hayfield Secondary's football and wrestling teams. Upon graduation, Kaleab decided to attend Old Dominion University to further pursue his interests in both engineering and wrestling. At Old Dominion, Kaleab was a part of the NCAA Division I Wrestling team where he competed for the Monarchs for four years. As he continued through his undergraduate coursework, his interests in mechanical engineering grew deeper and was presented with the opportunity to obtain a graduate degree through the accelerated program that Old Dominion offers and elected to continue with his education in hopes of completing his requirements and earning a Master of Science in Mechanical Engineering from one of Virginia's most prestigious programs. In his free time, Kaleab likes to relax and unwind with his friends outdoors. During

his undergraduate tenure, Kaleab held an internship position at Thomas Jefferson National Accelerator Facility where he worked in the mechanical engineering department for seven months leading up to his graduation in May 2019. Now, Kaleab is a full-time graduate student and graduate assistant working in the Mechanical and Aerospace department's tutoring laboratory.